Mixed effects regression for snow distribution modelling in the central Yukon

by

Andrew Benjamin Kasurak

A thesis
presented to the University of Waterloo
in fulfilment of the
thesis requirement for the degree of
Master of Environmental Studies
in
Geography

Waterloo, Ontario, Canada, 2009

Author's declaration

I hereby declare that I am the sole author of this thesis. This is a true copy of the thesis, including any required final revisions, as accepted by my examiners.

I understand that my thesis may be made electronically available to the public.

Abstract

To date, remote sensing estimates of snow water equivalent (SWE) in mountainous areas are very uncertain. To test passive microwave algorithm estimations of SWE, a validation data set must exist for a broad geographic area. This study aims to build a data set through field measurements and statistical techniques, as part of the Canadian IPY observations theme to help develop an improved algorithm. Field measurements are performed at, GIS based, pre-selected sites in the Central Yukon. At each location a transect was taken, with sites measuring snow depth (SD), density, and structure. A mixed effects multiple regression was chosen to analyze and then predict these field measurements over the study area. This modelling strategy is best capable of handling the hierarchical structure of the field campaign.

A regression model was developed to predict SD from elevation derived variables, and transformed Landsat data. The final model is: SD = horizontal curvature + cos(aspect) + log_{10}(elevation range, 270m) + tassel cap$_{greenness,brightness}$(Landsat imagery) + interaction of elevation and landcover.This model is used to predict over the study area. A second, simpler regression links SD with density giving the desired SWE measurements. The Root Mean Squared Error (RMSE) of this SD estimation is 25 cm over a domain of 200 x 200 km.

This instantaneous end of season, peak accumulation, snow map will enable the validation of satellite remote sensing observations, such as passive microwave (AMSR-E), in a generally inaccessible area.

Acknowledgements

I would like to thank my loving wife and partner of many years, Nicole, who has supported me through years upon years of school, and for getting me into geography, as no-one who maps a lake with a fish finder should be in any other program. To William, who will have to grow up with this world, so we'd better figure out how it works. To my parents for showing me the usefulness of higher education, and allowing me to explore it. Mr. Mike for convincing me to come to UW, with his POJDM ways. And the members of POJDM, without whom I should likely not be who I am.

My advisors Richard and Alex for advising me, with patience, and and support through the fieldwork, its exploration, and with my draft writing. They taught me of snow and statistics, and how the two might work together. You have allowed me to explore a whole new realm with a depth I could only dream of when I started.

And lastly, Claude and Chris, my thesis readers, who helped me turn this around in such a short time. Your willingness to lend an educated ear with little warning is heartwarming.

Table of contents

List of Figures

List of Tables

Chapter 1

Introduction

The measurement of snow water equivalent (SWE) over a region allows a number of important tasks to be undertaken such as water management for flood forecasting, and climate change studies. Estimation by remote sensing is ideal, as field sampling of the spatial distribution of snow over large areas is time consuming and expensive (Erxleben et al., 2002). In northern regions, passive microwave observations offer frequent repeat, wide area coverage at a scale suitable for regional management. Winter clouds and darkness do not interfere with measurements, providing information when it is most useful. For remote sensing measurements to be converted into geophysical variables, a data set for calibration must be obtained. Such data sets and validations exist for prairie environments, as well as modifications for tundra and boreal forests. It is known that the satellite measurements must be adjusted for the presence of forest, and small lakes.

In mountainous areas, field studies of snow distribution do not have sufficient extent to calibrate and validate an instrument which has a best case ground resolution of 6×4 km. Typical studies are done at the basin scale (Watson et al., 2006). The relationships developed between terrain attributes and snow depth (SD) or SWE at the basin scale may not be transferable to larger regions with different topographic and climatic characteristics.

This study aims to generate maps of SD, and SWE through a regression approach; the maps should be large enough in spatial extent to calibrate Advanced Microwave Scanning Radiometer - EOS (AMSR-E) sensor estimates of SD and SWE in mountainous regions for which no current validated data set exists (Derksen et al., 2007).

To meet this aim, a multi-level spatial sampling design is developed, and a suitable linear mixed-effects model for analysis and prediction of SD and SWE is constructed from field measured and ancillary geospatial data. The sampling scheme is designed to achieve a appropriate geographical coverage and reflect the variety of environmental conditions that control snow distribution, such as topography and land cover. It is further adapted to account for the logistic constraints and to the presence of local scatter and spatial autocorrelation.

1.1 Overview

This study is concerned with estimating how much snow is on the ground for all given areas in the study region, at a given time, from a temporally coincident field sample. Logically, there are two main factors that control how much snow is in a given spot on the ground: the amount of snow that falls, and the way it is (re)distributed. This study aims to understand the distribution of snow, assuming constant snowfall over the region. In a variety of similar regression type studies, the authors Anderton et al. (2004); Carroll & Cressie (1997); Elder et al. (1991, 1998); Erickson et al. (2005); Erxleben et al. (2002); Lapena & Martz (1996); Leydecker et al. (2001); Lopez-Moreno & Nogues-Bravo (2006); Luce et al. (1999); Molotch et al. (2005); Plattner et al. (2006); Stahli et al. (2002); Winstral et al. (2002); Trujillo et al. (2009) examine the regression relationship between SD or SWE and a variety of terrain factors including: elevation, slope, aspect, incoming solar radiation, land cover, wind (via shelter, or drifting). The produced regression equations are typically linear, with R squared of 0.78 to 0.98 and high variability. Sample spacing also ranges widely from 2 m to 250 m between individual measurements. Autocorrelation of SD (when reported) ranges from 18-30 m, and residual autocorrelation generally has a range of 250 m. SWE is frequently derived from a model of SD and a fixed or very simple relationship between depth and density.

1.2 Research objectives

There are three main objectives of this work. First, data gathering in its own right is important to increase the general store of arctic knowledge and facilitate other work. Second, from this data set an algorithm will be developed to calculate SD or SWE over a large area from a small number of measurements. Third, a spatial prediction, in the form of a map, of SD for 2008 and 2009 will be produced using this algorithm. This map can then be used in further work to validate remote sensing passive microwave (PM) snow estimates.

The quality of field measurements is of the utmost importance. To ensure the best possible final map, the measurements on which it is based should be as uniformly distributed in space[1] to minimize local bias. The autocorrelation distance of SD (and thus SWE) should be respected for ensuring sample independence (Cressie, 1991). All samples should be taken in as short a period as possible, to remove time as a predictive effect through snowfall or snowpack metamorphosis. Sampling should take place at the time of maximum accumulation to ensure a deep enough snowpack to be detectible by AMSR (>5-10 cm), but before melt, as wet snow is not well handled by current AMSR algorithms. To be of

[1] Or evenly distributed amongst a logical stratification of the sampling domain.

the most use, the resultant map should report a confidence interval for its predictions, and so should be made with statistically robust techniques.

The distribution algorithm should be simple and easily understood. As there will not be sufficient external data, or separated internal[2] data, to validate the algorithm (there exists only one other, very low count observation set for the same region, the Yukon Snow Bulletin data set (Janowicz, 2008)), it should be physically plausible and meaningful. It should have the smallest possible error on the fitting data, but at the same time not be overfit. A form of leave-one-out (LOO) cross-validation (CV) should therefore be performed to assess model performance and to detect overfitting.

The final snow map should be calculated at as close a scale as the observations to limit the effect of change of support problems (COSP). It can later be re-scaled for validation of satellite estimates.

1.3 Research significance

This research is important for hydrological management applications, such as water resource management, especially water impoundment schemes (for irrigation and power generation), which require knowledge of the amount of snow in storage, so that melt quantities, timings, and river levels may be forecast and managed. Furthermore, knowledge of the distribution of snow coupled with snow energy balances, as controlled by solar input, and the snow thermal regime enable robust prediction of snowpack melt volume and timing.

The central Yukon region is under-studied in terms of snow distribution due to the difficulty in accessing the field sites. While the Yukon snow bulletin maintains 56 observation sites in the Yukon, with 17 in the area of this study, these sites, by necessity, are sparsely

[2] A reserved portion of the field sample for verification would be ideal, but is expensive to obtain.

distributed, and are numerically insufficient to predict local-scale variations in SD or SWE.

This research contributes a valuable data set of SD, density, and structure over a large portion of the central Yukon. This data set, being available to the research community, can facilitate further hydrologic studies. The snow distribution algorithm and its methodology will contribute to the general literature and understanding of snow distribution processes. The use of mixed-effects regression combined with stepwise selection is unique in this field, and the concept has strong applicability to the efficient mapping of snow mass.

1.4 Thesis outline

This thesis presents the stepwise mixed-effects regression model for snow distribution in the central Yukon after first presenting the research context of snow distribution modelling (Chapter 2.4); an overview of the study site (Chapter 3); a description of the data collection methodology (Chapter 4.3); and details on the processes of performing the stepwise mixed-effects regression (Chapter 4.3.4). The modelling results are presented in chapter 5. Finally, the implications, limitations, and recommendations will be discussed in chapter 6.

Chapter 2

Research context

To model how snow is distributed on the landscape, the processes which govern it must first be described. These processes suggest topographic and vegetation influences which should be examined as candidate variables in any snow distribution model.

2.1 Snow distribution

The distribution of snow over an area is best conceived of as a chain of processes, starting with snowfall and deposition onto the ground surface or vegetation. After snow accumulates on the ground, a number of processes act upon it, including redistribution, metamorphosis, and loss. The combination of these processes lead to the final snow distribution.

2.1.1 Snow deposition

Snow deposition is snowfall which has made it to the ground. There are several factors which control snowfall: weather conditions, topography, and surface land cover type. Weather controls humidity, and temperature, and also determines the paths of snow storms which influence the total amount and distribution of snow that falls in a given region. Topography controls relative humidity through orographic precipitation, and temperature by means of the lapse rate. Land surface cover contributes to accumulated snow by effecting wind speed through vegetation promoting deposition and preventing scouring; by intercepting falling snow; and at a large scale, by increasing available moisture (humidity) through evaporation over waterbodies.

Coniferous trees, which keep their needles in the winter, have a good ability to capture (intercept) snow as it falls. Snow in this canopy acts differently from snow on the ground. It is more vulnerable to sublimation, and acts in closer concert with the air temperature and moisture regime. Also, snow in the canopy will not immediately reach a snow gauge, inducing a measurement delay or bias. While in the canopy, snow is much more accessible to the atmosphere, having no ground under it, and no snow surrounding it. This lowers the temperature gradient inside the snow, an important factor for metamorphosis, and vastly increases the rate of sublimation, due to access of air. Rates of loss to sublimation range from 25–50% for coniferous canopies, with differences by author (Montesi et al., 2004). Research to model the snow capture of various canopies has been made (Hedstrom & Pomeroy, 1998), with an R^2, the coefficient of determination[1], between measured and modelled interception of 0.83 in jack pine, and 0.97 in black spruce with low standard errors. In addition, snow can be transmitted to the ground after a period of storage, as a result of melt, branch unloading, or wind redistribution, arriving at the ground in a different form than when it fell. This may further bias precipitation measurements, as this does not represent a precipitation event. Vegetation can intercept falling snow by

[1]This measure for the quality of the regression is sub-optimal and may not be used to compare studies, as it is highly dependent on the distribution of sample data. RMSE and the Coefficient of Variation would be more helpful, but are less frequently reported.

physically catching it upon its branches, or by having it touch and adhere to already intercepted snow (Hedstrom & Pomeroy, 1998). As snow collects on a branch, it first fills the smallest spaces between needles (or leaves or branches), forming bridges (Pomeroy & Gray, 1995). These enhance the ability of the branch to collect further snow. Collection efficiency decreases after the branch fills, as new particles bounce off the curved surface of the snowpack. Collection efficiency is also strongly affected by temperature, warm temperatures increase cohesion, but also allow branch bending (and therefore unloading), and weaken the snow structure through metamorphism (Pomeroy & Gray, 1995).

2.2 Snow redistribution

Wind is a key factor in snow redistribution through entrainment of the snowpack, losses of snow by enhancing sublimation, and compaction of snow through the application of force. Both wind speed and direction are needed to properly model the effects of wind on the snowpack. Other atmospheric variables such as relative humidity and temperature will influence the effects of wind on snow. Wind speed is critical, as there is a certain threshold wind speed for a given snowpack, below which the wind will not have enough force to entrain particles. Once this entrainment velocity is reached, particles will begin to saltate (creep may begin at a lower speed).

Wind which flows over vegetation imparts a portion of its force to the vegetation as a sheltering effect, and a portion to the surface, allowing snow to fill up to the vegetation height, and erode only after this, excepting in particularly strong wind conditions (Pomeroy & Gray, 1995).Shelter acts by reducing the boundary layer wind speed, and thus the ability of the wind to overcome the threshold friction velocity of the resting snow (Pomeroy & Gray, 1995), in the same manner as to soil (as seen by Lyles & Allison (1976)).

A variety of site-specific studies of snow transport,as done by: Pomeroy et al. (1993); Li & Pomeroy (1997); Essery et al. (1999); Leydecker et al. (2001); Liston et al. (2007), and others, using models and *in situ*data show significant losses of snow due to sublimation during transport. Pomeroy & Li (2000) cite a ratio of losses of 2:1 (prairie), and 1:1 (arctic) for sublimation : transport during transport events. The rate of sublimation is related to the loss of water vapour from the surface layer, as estimated on a spherical particle. The physical controls are (Pomeroy & Gray, 1995): radius of the sphere, diffusivity of water vapour in the atmosphere, degree of turbulent transfer of water vapour from the particle surface to air (Sherwood number), water vapour density of the ambient air, water vapour density at the particle surface. These can be combined by integrating over the height of the snow column to provide an estimate of the sublimation loss.

2.3 Snow metamorphism

Deposited snow does not remain static, immediately beginning metamorphism. Snow compacts by breaking individual crystals into more regular shapes, it can loose water to melt or sublimation, or gain water from vapour fluxes from the soil (Pomeroy & Gray, 1995). It may also be changed by surface processes creating melt-freeze crusts, hoar, or ice lenses.

In general, the snowpack becomes denser, and more resistant to erosion by wind. Grains become rounded, and joined together -'sintered'. Average density[2] rises from approximately 100 kg / m^3 to the range of 200–350 kg / m^3; and upwards of 500 kg / m^3 when melt is underway.

When a thermal gradient exists between the soil and the top of the snowpack, water

[2]The density of snow, both as it falls, and as a result of metamorphism, depends on many factors, and is quite variable.

vapour will move from the warmer to colder regions in the snow/ground/air system. This causes an upward migration of water, as the ground is usually warmer than the overlying snow and air during winter. When this water vapour refreezes, it has a different crystal structure, known as hoar (either depth hoar in the pack, or surface hoar as a crust). This form contains more water than the untransformed snow, in larger grains; and is structurally, as a snowpack, physically weaker (Pomeroy & Gray, 1995). When the soil is the source of moisture, a layer of depth hoar can form which significantly reduces the strength of the bottom of the pack and its adhesion to the ground surface. This can lead to instabilities such as avalanches. Pomeroy et al. (1993) suggests that the majority of water vapour movement occurs within the pack, rather than as vapour escape to the atmosphere.

Incoming radiation acts upon the snowpack to melt it, increasing variability of the resultant SWE distribution (López-Moreno et al., 2007).Luce et al. (1998) discusses the impact of incoming radiation on net accumulation through a distributed energy balance model. Partial melting during the daytime may form surficial features such as sun-cups (small melt spots), and penitentes (tooth-like pillars)[3] which create lower albedo, and shadows, respectively (Herzfeld et al., 2003).

2.4 Modelling snow distribution

2.4.1 Physical models

Physical models attempt to simulate snowfall and redistribution using physically based mass and energy balance processes and parameterizations of snow. They require a large

[3]Penitentes occur in regions where the dew point remains below zero, and sublimation is the dominant process (Corripio & Purves, 2005). These regions were not found in the study site, but may be present in the unreachable permanent snow.

number of inputs for meteorological data which are updated over the model run. To model maximum accumulation at the end of the season, it is necessary to start from a known initial state (such as pre-snowfall of 0 mm SWE) and simulate the whole accumulation season. Blöschl (1999) describes parameterization as necessary for any process which occurs at a scale below that of the model. In distributed models (such as in the Prairie Blowing Snow Model (PBSM (Pomeroy, 1989)) variants Distributed-BSM and Simple-BSM), and SnowTran-3D (Liston & Sturm, 1998) the scale is much larger than that of the processes of sublimation and saltation, therefore these processes are parameterized. Parameterization can benefit a model by simplifying a process, resulting in faster calculation, or by abstracting away portions that are not well understood. Simulation accuracy depends on the spatial distribution of the meteorological data, as well as the correct parameterization of processes. This is not suitable for the study area in this work as it is a very large area, and contains very sparsely distributed meteorological stations (an exception is Liston & Sturm (2002), where SnowTran-3D is used to transform snow depth measurements over a 85x230 km area including the Kuparuk river basin in Alaska, at 100 m resolution, into a distributed precipitation map). Larger scale climatic models can predict snow depth, but do not give fine resolution prediction maps, and thus may miss the local-scale spatial variability of the snow distribution.

The advantage to physical models, which properly model the phenomenon of interest is the production of plausible results when presented a novel situation. The second main advantage addresses a major limitation of this study, field access. Since the model inputs are meteorological, rather than survey based, less distributed access is required to map snow. The disadvantages is three-fold: firstly, physical models are more complex, and take a significant amount of time to process the data, which must exist from a known state, through a continuous measured period. Secondly, the process must be well understood and mathematically modelled. The effectiveness of the choice in model scale will have a large influence, as all key processes should be at or above the model scale, to avoid parameterization, by which the physical simulation advantages are lost. Thirdly, the input requirement of meteorological data from field stations is not simple to obtain, or to distribute over the study area. Liston & Elder (2006) describes a meteorological distribution approach. Meteorological stations are expensive, and prone to failure in cold climates.

- PBSM focuses on the redistribution of snow over an abstract land unit, based on physical processes and local meteorological data. The goal is to calculate the amount of snow in a given land unit, at any time after initialization. It considers the flow of blowing snow over a point (Figure 2.1a), taking into account the upwind fetch, and the surface roughness from vegetation. It has been extended to model an area, as DBSM; and has also been simplified by statistical summation of probabilities as SBSM. The focus is on the accurate modelling of the processes involved with the movement of snow and its loss due to sublimation. It has been applied to open and shrubby tundra environments.

- SnowTran-3D (Liston & Sturm, 1998; Liston et al., 2007) (ST3D) is a distributed model, developed by Liston and Sturm from the initial concept of PBSM, but with a more complex representation of terrain and its effects on wind speed. By allowing for wind to accelerate and decelerate based on convergent and divergent terrain forcings, the ability of the wind to scour and transport snow is spatially variable, and better models snow distributions in complex terrain. The 2007 version (2.0) includes further generalization and more detailed sub-models for wind, physical snow properties, and snow drifting. It also has a linked model to distribute meteorological data, and interpolate missing observations. In addition, it is now adapted for alpine areas. The basic concept of ST3D is presented in figure 2.1.

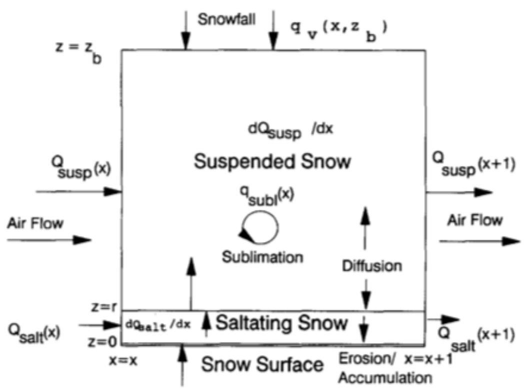

(a) PBSM

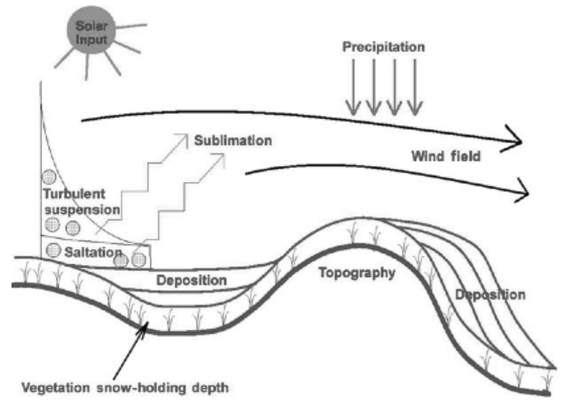

(b) SnowTran-3D

Figure 2.1: Conceptual 2D snow transport. PBSM from (Pomeroy et al., 1993, fig. 4), SnowTran-3D from (Liston & Sturm, 1998, fig. 1)

2.4.2 Statistical models

Statistical models predict values for a region based on a spatial sample of related variables of interest. They do not rely on any thoroughness of understanding of the underlying physical process of snow distribution, so long as the correct variables are observed. However, forecasting with an observational statistical model is not recommended, as the model will not react to external forcings such as climate or meteorological processes, if they were not directly included in the model.

Table 2.4.2 (see also table 6.1) is compiled from a number of regression based studies which predict SD or SWE from terrain and land cover variables. The following commonalities are observed: 1) The regression is usually linear, with SD as the response variable, due to its ease of measurement. 2) Elevation, slope, aspect, and incoming solar radiation are the most common variables to be included as predictors. Landcover is less frequently used, and generally only as a a marker of forest density. 3) The resulting statistic, R^2, varies widely, from 0.1 through 0.9[4]. The majority of authors have confidence that their studies accurately, if not precisely describe the snow distribution observed. 4) Wind as a variable is less frequently used, and is generally in the form of shelter. This is frequently due to the lack of wind speed and direction measurements. 5) The range of spatial autocorrelation (SAC) is similar in all studies, irrespective of location or year. Marshall et al. (2006) investigates a number of datasets for autocorrelation range and makes a similar conclusion, in addition noting that magnaprobe estimates show more variability than fine scale radar, due to point support. Fassnacht & Deems (2006) also concludes the response-level autocorrelation range for the CLPX[5] snow depth data set is 15–40 m, and suggests sampling at approximately half that if the small scale structure is important, otherwise 30–100 m, although study areas above 1000 m were not considered.

[4]Studies based on small, homogenous regions may have a poorer R^2, as the sampling domain for the homogenous variables may be within the variability of this variable

[5]NASA's Cold Land Processes Experiment (CLPX) was a extensive multi-temporal, multi-sensor field campaign in Colorado in 2002 and 2003. The data is available from the National Snow and Ice Data Center (NSIDC)

Regression studies

Study	Area size	Regressors	SAC
Anderton et al. (2004)	0.32 km^2	SD = E + R*+ S* + W exposure at 7–49 m (37*)m	N/A
Carroll & Cressie (1997)	10625 km^2	SWE = S + A + E* + tree cover	N/A
Elder et al. (1991)	1.2 km^2	SWE(from SD and some density measures) = E* + R* + S*	N/A
Erickson et al. (2005)	2.3 km^2	SD = E + S + R + W	250 m**
Erxleben et al. (2002)	3x 1 km^2	SD = E + S + A + R + type and density of V (trend model varied in included terms between each sub-site, all variables appeared at least once.)	18 m
Jost et al. (2007)	17.4 km^2	SWE=E* + A* + V* + R + S + Temp	<10 m
Lapena & Martz (1996)	1.5 km^2	SD=E* + S* + C + W* + V*	N/A
Leydecker et al. (2001)	19 km^2	SWE by SD = E + R + S + A	<30m
Lopez-Moreno & Nogues-Bravo (2006)	47452 km^2	SWE by SD = E*+ S + A + R*+ elev_rng(calculated at various ranges, as was slope, and radiation)+ dist:ocean, dist:divide*	N/A
Molotch et al. (2005)	19.1 km^2	SWE by SD = E + S + A + R + W	N/A
Plattner et al. (2006)	8.36 km^2	SWE by SD = E* + S + A + W* + C*+ dist_ridge*	250 m**
Stahli et al. (2002)	0.75 km^2	SD = E + V (via: Tasseled cap (bright, green, wet), NDVI, simple ratio 7/5,4/3, 4/2) +R	500 m** +
Winstral et al. (2002)	2.25 km^2	SD = R* + E* + S* + W*	N/A

Table 2.1: Findings of similar studies (also see tables 1 and 6 in Erickson et al. (2005) for further models. Abbreviations in this table: SAC: spatial autocorrelation, E: elevation, S: slope, R: incoming solar radiation, A: aspect, W: wind, V: vegetation, C: curvature. *: Items included in the final model. +: a value as low as 25 m might be estimated from the graphs presented. **: residual. The studies by Elder et al. (1991); Molotch et al. (2005) take place in the same basin as Leydecker et al. (2001)

Considering the forms that a statistical model might take, there are a few choices that are widely used in the literature. These are: regression modelling (linear and non-linear regression, mixed effects regression), generalized additive models, binary regression trees, and kriging (universal, ordinary, and co-kriging).

A regular (fitted with ordinary least squares) regression model was unadvisable for the collected data set, as there will be significant spatial autocorrelation between samples in the same site, and sites in the same transect due to the nested structure. This violates the assumption in linear regression of independent samples. This factor is not frequently discussed in the papers which use linear regression models. Nonetheless, regression has the advantage of being simple, and of modelling the impact of a variable directly, over its whole range.

Binary regression trees are less useful as they are unable to produce a continious surface. The number of levels of the predicted variable is tied to the number of levels of the tree. A deeper tree with more levels will be more likely to be over-fit (Lopez-Moreno & Nogues-Bravo, 2006), while few levels produces less detail in the result. In addition, binary trees do not model the effect of the whole range of a variable, relying only on selected breakpoints in the measured empirical relationships, so may not be as transferable as they cannot extrapolate beyond observed ranges (Lopez-Moreno & Nogues-Bravo, 2006), and will be sensitive to an interaction causing a shift in the breakpoints. Binary trees have the advantage of inherently modelling interactions, and non-linearities, and will focus on the most significant[6] (Breiman et al., 1984) breakpoints in the observed data set, thus implicitly selecting the most influential candidate variables for inclusion in the final model.

Kriging is a Best Linear Unbiased Predictor (BLUP) for a spatial variable (Cressie,

[6]significant, in terms of the split providing the largest reduction in node impurity in the two created leaf nodes, not globally.

1991). Like Inverse distance weighting (IDW) the distance to the measured location is used to interpolate, however, unlike IDW, the structure of the randomness with which the variable is distributed is used to control the interpolation. Using a trend surface (as in ordinary or universal kriging) to incorporate regression into the kriging process is typical. The distribution of sparse sampling points in the field data set renders kriging unadvisable, as the points are not evenly distributed over the whole of the study area. Co-kriging against a uniformly sampled variable is possible, using information about cross-correlations between snow and other predictor variables, but only if the model for autocorrelation is of similar scale. Universal co-kriging would have been more viable if the existence of strong relationships was known before the sampling was undertaken.

Generalized additive model (GAM) are a form of semiparametric regression where, rather than specifying a non-linear term, the model fitting includes an optional smoothing step where a function (smoothing curve) is fit to the data (Faraway, 2006). This gives the model great flexibility in dealing with non-linear relationships, and removes the need to transform predictor variables to linear relationships.

Linear Mixed Effects Regression(MER) models combine a structure of 'fixed' effects, as in linear regression, and 'random' effects which allow subject-specific fitting. In addition, the random effects structure allows for hierarchical structure, and these grouping factors to have separate variance structures, and within-group correlations. This specification accommodates the non-independence of spatial sampling within the autocorrelation range, and within nested levels. For this study, a grouping factor based on the sampling scheme was the simplest approach.

$$y_i = \alpha + \mathbf{X}_i\beta + \mathbf{Z}_i\mathbf{b}_i + \epsilon_i, i = 1, \cdots, N \tag{2.1}$$

A MER model has two components (Equation (2.1)): fixed effects and random effects (Demidenko, 2005). Fixed effects (β), and the intercept α, are the standard regression covariates. Random effects ($\mathbf{b}_i$) are population parameters which affect the distribution of the variable through the covariance matrix, $cov(\mathbf{b}_i) = \sigma^2\mathbf{D}$, but which will not necessarily be used calculate a direct relationship. They must have a mean of 0, and are independently and identically distributed, and $\mathbf{Z}_i$ is the design matrix. In a multi-level model, they must also be used specify a grouping structure (Pinheiro & Bates, 2000). The i's are the observations, of which there are N. The variance parameters, σ^2 and $\mathbf{D}$ are not known, and are part of the model estimation (using maximum, or restricted maximum, likelihood) of the fixed effects portion of the regression (the β's) . Heteroscedastic errors and other modifications such as spatial autocorrelation can be added into this formula.

Using the sampling structure as a random effect partitions the resulting lack of fit variance into the sampling levels. While this information is unavailable to prediction (it is not known which transect a new point belongs to), it aids in the understanding of the SD variability.

Testing a MER model can be undertaken on either the fixed or random terms. Fixed effects may be tested with t or F tests (conditional on the estimated variance), as likelihood ratios tend to be anticonservative (Pinheiro & Bates, 2000), although correction is possible through empirical simulation. Random effects specifications may be compared between models if they are fitted with the same fixed effects specification (Pinheiro & Bates, 2000).

MER modelling has been used by López-Moreno & Stähli (2008) to account for interannual variation in a multi-year data set. In this study, the year was a random effect, and forest presence, altitude, and potential incoming radiation were fixed effects. No fixed effects selection procedure was used during the model fitting, instead terms were selected by literature search. The sampling design incorporated measurements at 1 m separation over 30 m linear transects. Measurements were manually aggregated to the transect level, as no random effects were used as a grouping structure. Five density measurements were made per transect, and the average SWE was calculated and used as the model response.

2.5 Summary

In this chapter, two types of models have been described: physical models that model end of season accumulation of the snowpack as the net effect of meteorological inputs and hydrological processes over the whole season, and empirical statistical models which model SD by spatial prediction from a set of field observations. A statistical approach was chosen for this study as the best means to get an instantaneous end of season accumulation picture for the purposes of passive microwave validation. While a physical model is preferable in understanding the phenomenon and adaptivity to changing conditions, the lack of required meteorological inputs over the study area prohibits their use.

The best choice of statistical model for the region is the linear mixed-effects model. It has the advantage over other regression approaches by including the structure of the observations, and thus the implicit autocorrelation. It does not suffer the trade-off between resolution and over-fitting of a tree model, and it does not have the spatial distribution requirements of kriging.

Therefore, the objectives of the study shall be to fit a MER model for SD and SWE, and to produce from this a predicted map over the central Yukon. Using the design of the MER will allow for the sampling structure most easily performed (many observations grouped, rather than a true random sample).

Chapter 3

Study site

The study area is located in the upper portion of the Yukon river watershed, incorporating portions of the Yukon headwaters, Pelly river, and upper Yukon river drainage basins. The Yukon river basin is very large (4th largest in North America) covering most of the land area of the Yukon, and drains to Alaska, in the north-west.

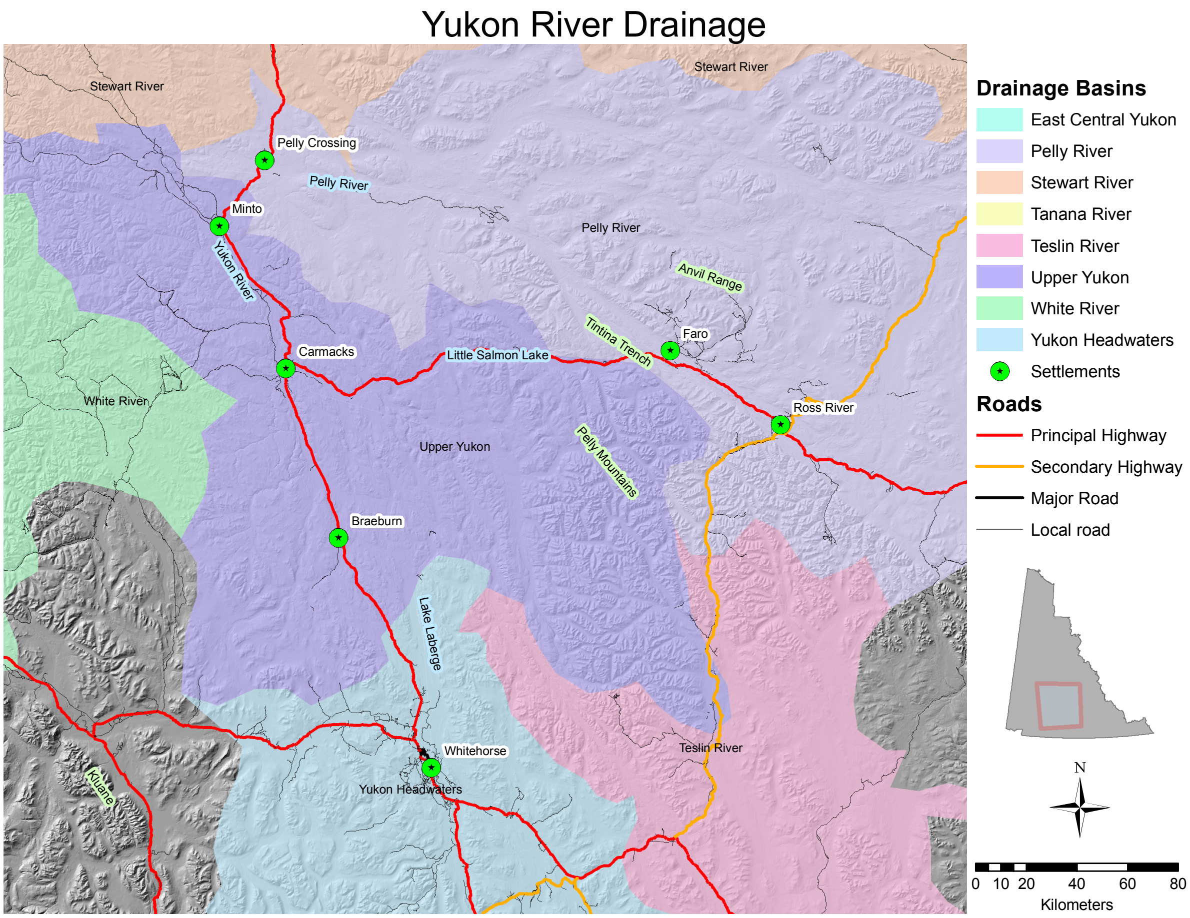

Figure 3.1: Field location in the central Yukon

3.1 Local site

The study area encompasses the region from Whitehorse in the south to Carmacks, approximately 200 km north along highway 6 and the Yukon river, then to the town of Ross river, 200 km east of Carmacks on Robert Campbell highway (highway 4), along the Ross river. The study area includes two large lakes, Lake Laberge, aligned N-S, and Little Salmon Lake, E-W, as well as numerous small lakes. Permafrost is sporadic for the majority of the study area, becoming discontinuous on the north and west edges (Brabets et al., 2000).

3.1.1 Morphology

The Yukon is mountainous with elevations ranging from sea level, to Canada's highest peak, Mt. Logan at 5959 m. In the study area, elevation ranges from 504m to 2222 m. The Tintina trench, a large rift valley 5–19 km wide with an average elevation of 600 m a.s.l., runs NW-SE bordering the Pelly mountain ranges on its western flank.

Brabets et al. (2000) describes five general physiographic regions which are present in the Yukon river basin: 1) rolling topography and gentle slopes, 37 percent; 2) low mountains, generally rolling, 24 percent; 3) plains and lowlands, 20 percent; 4) moderately high rugged mountains, 17 percent; and 5) extremely high rugged mountains, 2 percent.

3.1.2 Elevation

The distribution of elevation is shown in figure 3.2a. The maximum sampled elevation in the field data was 1392 m, which covers the majority of the elevations found in the study area, with the exception of the high peaks.

3.1.3 Vegetation

Vegetation is dominated by white and black spruce on dry and wet soils respectively. Lodgepole pine is common as regrowth and on very dry areas. Aspen dominates burn regrowth and south facing slopes, birch and dwarf willow are also common. The tree line occurs around 1500 m. Details on the distributions of topographic variables are described in table 4.4, and more information on the region in Brabets et al. (2000).

The relative distribution of classified land covers can be found in figure 3.2b. For the purposes of this study, both bare and burn areas were combined, as bare areas were only encountered in one field site (the highest elevation site). The bare site examined was

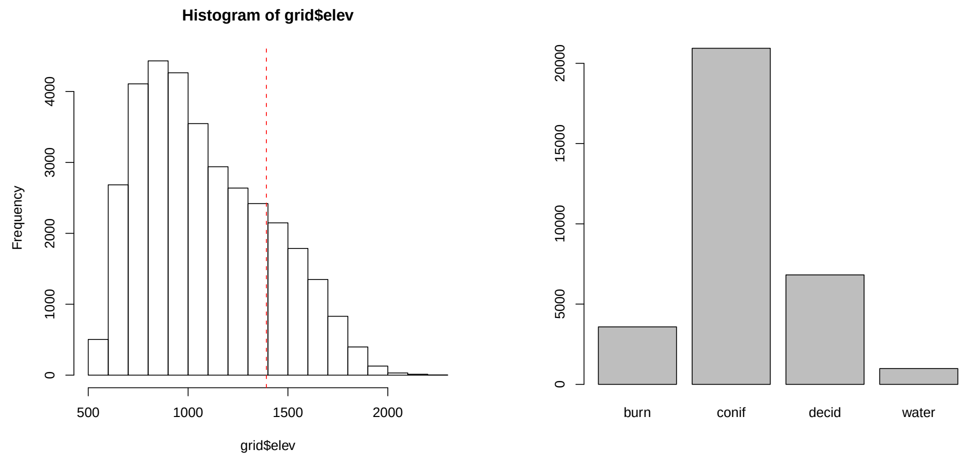

(a) Histogram of elevation. (b) Histogram of vegetation classes.

Figure 3.2: Frequency of (a) elevation and (b) land cover (vegetation) over the whole study site. Elevations between the dashed line were sampled in this study. Vegetation categories are explained in chapter 4.1.

typified by boulder fields, sparse vegetation and other rough surfaces which made it more similar to the burn site than to water, which was the other option to combine with. On page 53, a distinction between the two classes will emerge with the $isforest$ variable.

3.1.4 Climate

The central Yukon is a generally cold and semi-arid climate. Mean annual precipitation the the study area is approximately 254-381 mm per year, with a relatively uniform distribution (Brabets et al., 2000). Wind in the study area is of two components, an unrestricted above-valley flow generally from the west, and a within-valley flow generally parallel to the valley direction (Pinard et al., 2005). Winter winds are typically stronger than in summer for the mountaintops, but the reverse is true for valley bottoms.

The snow season for 2008 was an above average SWE (111–130% normal SWE) year

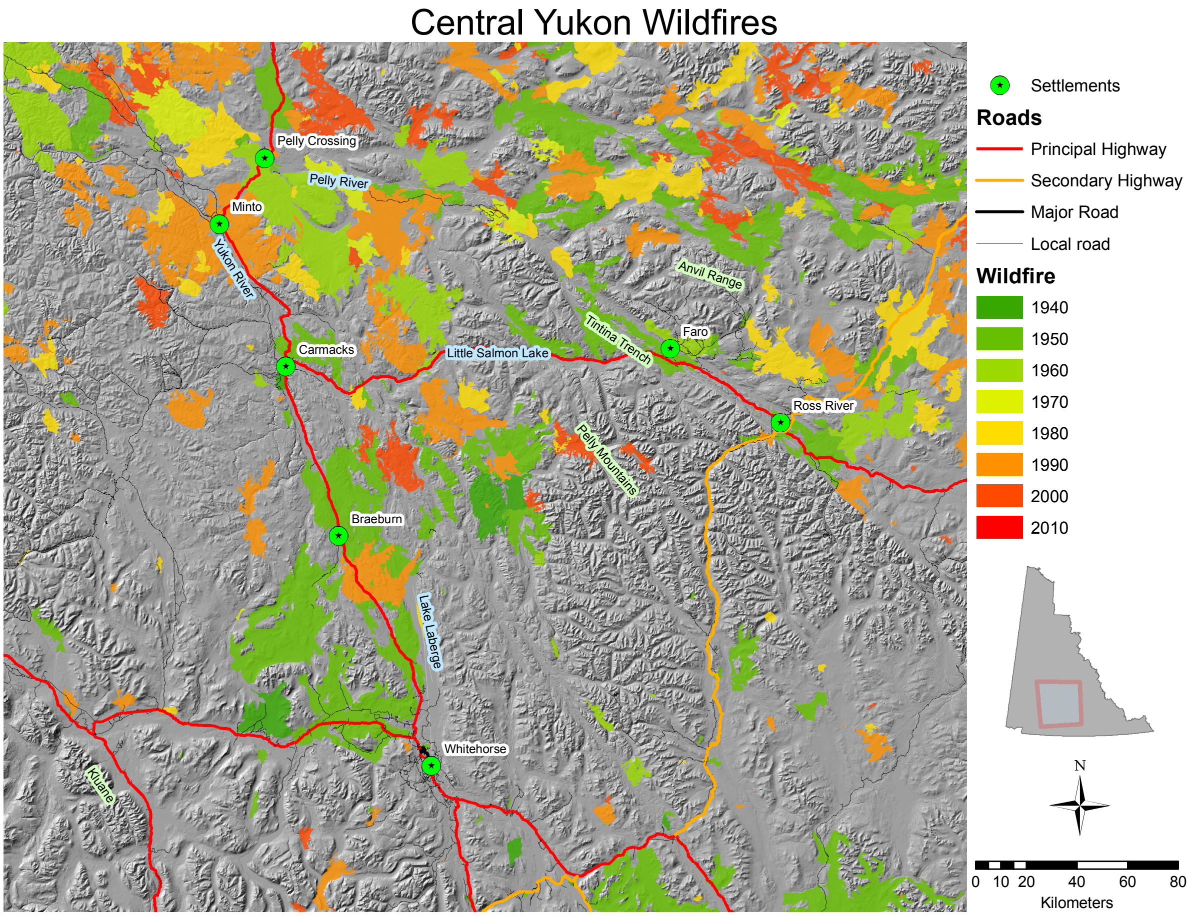

Figure 3.3: Wildfires and regrowth areas in the central Yukon (Brabets et al., 2000).

in the study area, according to the Yukon snow bulletin (Janowicz, 2008), which observes snowpack conditions at 56 snow pillow and transect sites spread over the central Yukon. Temperatures averaged about 2°C higher than normal, and precipitation was only about 75% of normal[1].

The snow season for 2009 was also above average (130–150% normal SWE).

[1]The difference in observed precipitation and SWE accumulation may be due to measurement error, however no details are available. The SWE measurements should be taken as having stronger support, as they are not as susceptible to unnoticed instrument failure.

Climatic SWE by year

Basin	Mean	1-apr-08	1-apr-09
Upper Yukon	200	250	275
Whitehorse	125	130	200
Pelly River	150	175	210

Table 3.1: Climatic SWE conditions (mm SWE) (Janowicz, 2008). Mean data based on records of 5–50 years.

3.2 Summary

The study site is a large region of foothills and mountains in the central Yukon, approximately 200 km north and east of Whitehorse. The landcover is mostly coniferous dominated boreal forest, but at higher altitudes, and in forest-fire regrowth areas deciduous trees compose the majority of the population. During both study years, an above average accumulation was recorded, although to a different degree and distribution in each year.

Chapter 4

Methods

Mixed effects regression modelling provides a useful adaptation of the regression methods to a hierarchical data structure, such as one obtained by an observations within transect sampling strategy. Before a model can be built, both the predicted and predictor variables must be enumerated. The model construction should attempt to assess and correct any violations of assumptions within the MER framework, namely that of the structure of within group and residual errors. A good model will be parsimonious and have predictive power, therefore model selection should incorporate a measure for each.

The first step in performing a regression was to choose the predicted variable. Two choices were available: SD and SWE. SWE is derived by combining SD and snow density, which was measured with a lower frequency than SD, causing SWE to be smoothed. However, since density was not uniform over the whole study area additional information might gained by including density as SWE prior to regression. The simpler approach of modelling SD first, and converting to SWE through a second regression was chosen so as to produce the best possible results. Having both a SD map, and a method to convert to SWE allows the qualities of both to be used: the increased accuracy of the repeat observations of SD should create a more accurate SD map, leaving the uncertainty from the less-frequently sampled data in a separate model.

4.1 Variables

To summarize the characteristics of the study sites, a number of terrain attributes are calculated. A 90 m digital elevation model (DEM) was acquired from Geomatics Yukon. From this, slope, elevation, aspect, and curvature (plan, profile, 3D) were derived in the System for Automated Geoscientific Analyses (SAGA) GIS program. Aspect was transformed to both sine and cosine to facilitate linear regression analysis. Positional information from the Magna-Probe allowed the ancillary information to be tied to the field data (via SAGA GIS and RSAGA package for R (Brenning et al., 2008)). The following description explains the terrain variables (summarized in table 4.3 and table 4.4) considered for inclusion in the model.

Variables derived from DEM

- Elevation (*elev*): Height above sea level in meters.
- Elevation Range (*elev_rng*): The range of elevation change (max-min) within a radius of 3 pixels (270 m)[1]. This variable is similar to slope, but is calculated using information from a larger local area.
- Elevation Standard Deviation (*elev_stdev*): The standard deviation of all pixels surrounding the location within a radius of 270m. A measure of roughness. Values are in meters.

[1]As measured with the circular radius tool in ArcMap

- Slope (*slope*): Instantaneous slope at the location, in radians.
- Aspect: Sin, Cos, Factor (*aspect_sin, aspect_cos, aspect_fac*): Aspect of slope, measured in degrees from north, clockwise, decomposed into sine and cosine components, so as to remove the circularity of the number and allow for linear regression. Flat areas are assigned a value of -1 by the geoprocessor. To allow for proper incorporation of these values into the regression, aspect was classified into eight 45 degree groups (N, NE, E, SE, S, SW, W, NW), and one additional group for flat areas. Both sin/cos and factorial transformations were considered for inclusion.
- Curvature: V, H (*vcurv, hcurv*): The shape of the hill-side, as both horizontal (plan, cross-slope), and vertical (profile, down-slope) curvature components, in radians per meter.
- Incoming radiation (*solrad*): Net incoming radiation from 1 january to 31 march, assuming clear sky. Calculated as the sum of short and longwave radiation, taking into account the slope of the ground, and elevation. As described in Wilson & Gallant (2000), and implemented in SAGA GIS. Units are in Watt hours per meter squared. Incoming radiation in this study is vastly simplified, and will be remarked upon in the further work section, 6.4.
- Position: (*Lat, Lon; x, y*): Measured in the WGS84 coordinate system, NAD83 datum. Reported in decimal degrees. Transformed to Albers equal area conic, units (x, y) in meters.

Variables derived from imagery

- Normalized Vegetation Difference Index (*NDVI*): This index is derived from the red (RED) and near infra-red (NIR) bands of visible imagery RS. It detects vegetation health, and can be related to leaf area index (Jensen, 2007). The formula is shown in equation (4.1). Values are rescaled to 0–255, rather than the normal -1 to 1.

$$NDVI = \frac{NIR - RED}{NIR + RED} \tag{4.1}$$

- Tasseled cap transformation (*ts_{bright, green, wet}*): is a principal-component decomposition with pre-determined coefficients (Jensen, 2007). The three primary components are brightness (*ts_bright*), greenness (*ts_green*) and wetness(*ts_wet*), respectively. Brightness is useful for detecting soil and urban areas. Greenness is similar to NDVI, and wetness detects water and vegetation. Both of these transformations work on a per-pixel basis, rather than with global statistics, reducing the impact of changing mean brightness levels or seasonality between different scenes (Jensen, 2007). The equations for the tasselled cap transformation are shown in equation (4.2), where $TM_{\#}$ stands for Landsat Thematic Mapper band #. There are further principal components available, but are less commonly used, and were not used in this work. Values are in digital number (DN), 0–255.

$$B = 0.2909TM_1 + 0.2493TM_2 + 0.4806TM_3 + 0.5568TM_4 + 0.4438TM_5 + 0.1706TM_7 \tag{4.2a}$$

$$G = -0.2728TM_1 - 0.2174TM_2 - 0.5508TM_3 0.7221TM_4 0.0733TM_5 - 0.1648TM_7 \tag{4.2b}$$

$$W = 0.1446TM_1 + 0.1761TM_2 + 0.3322TM_3 + 0.3396TM_4 - 0.6210TM_5 - 0.4186TM_7 \tag{4.2c}$$

- Supervised classification (*lc_sat*): A supervised classification (figure 4.1) of the scenes was undertaken. Each scene was individually processed. For each land cover class of: Deciduous, Coniferous, Water[2], Burn, Ice & Cloud, pure pixels were selected, at least 100 each. A hard classifier was used, and no mixed pixels or unclassified pixels were permitted.

  A classification assessment to determine the best classification algorithm was performed on landsat scene 59–17, which contained the majority of the field observations, by comparing classified values from the same selection of pure pixels. Parallelpiped, minimum distance, mahalanobis distance, and maximum likelihood derived classifications were compared against the field observed land covers. In addition, the capability of each classifier to deal with difficult situations, such as mountain shadow[3], was quantitatively graded. The results of this are presented in table 4.1. Ground truth values were derived from field sites visited. On the ground many sites contained a mix between deciduous and coniferous, making a hard classification difficult. This will limit the maximum accuracy reported of the classifications.

  In table 4.1, the minimum distance classifier was chosen as the best performing classifier, and was run on the available imagery. The minimum distance technique uses the mean vectors of each endmember and calculates the Euclidean distance from each unknown pixel to the mean vector for each class. All pixels are classified to the nearest class unless a standard deviation or distance threshold is specified, in which case some pixels may be unclassified if they do not meet the selected crite-

[2] The classification was performed on a summer image, so Water class pixels would be Ice in the field classification. The Ice class pixels in the classified image are year-around ice features such as glaciers.

[3] A topographic normalization could have been performed, but was judged unnecessary due to the lack of field data in the higher mountains where this problem is most frequent. Should the field domain extend higher, this will require action.

ria (ENVI Help). The classification procedure was run on each scene, using all 30 m untransformed bands, and the results mosaicked together.

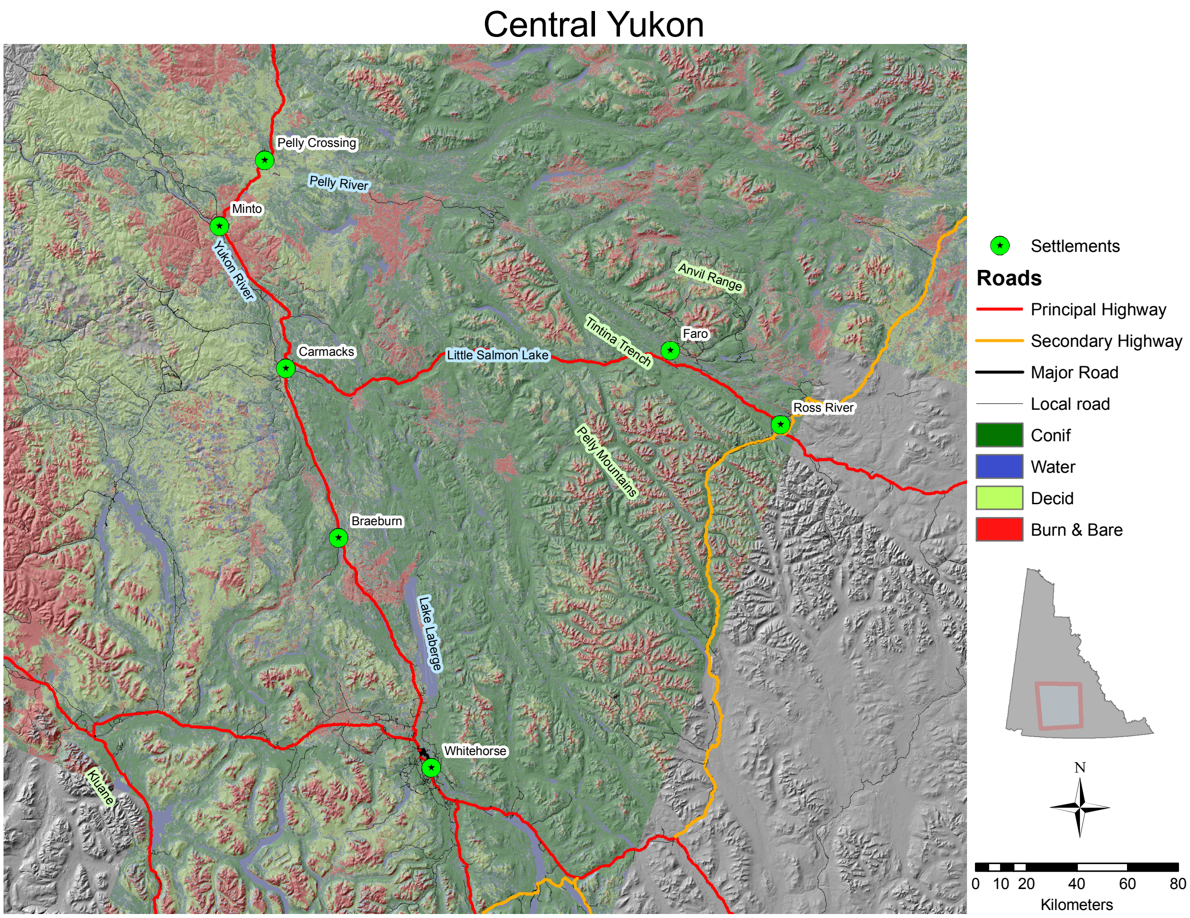

Figure 4.1: Classified land cover.

Landsat classification assessment

Method	% correctly assigned	qualitative
Parallelpiped	42	Poor
Minimum distance	73	Best
Mahalanobis distance	71	Good
Maximum likelihood	51	Poor

Table 4.1: Landsat classification assessment by comparison with field observations, and qualitative ranking of edge and shadow effects.

4.2 Available data

4.2.1 Elevation data

A 90 m digital elevation model (DEM) was acquired from Geomatics Yukon (B.2). This DEM covers all of the Yukon. A 30 m DEM was available, but not mosaicked. Mosaicking a DEM introduces many edge effects, and thus would add either errors, or undue work[4]. Geomatics Yukon has already performed error checking on the 90 m product.

4.2.2 Imagery

Landsat imagery was acquired from the USGS EarthExplorer data portal, and the Yukon Geomatics data portal. When different years had to be selected for cloud free imagery, the same month was sought. All imagery was from 1999–2001, and may thus not exactly match the field information in areas where forest fires have since occurred.

Mosaicking: All suitable images are first mosaicked, combining them into one image. All images contain georeferencing information, and are reprojected into a common system (Albers equal area conic) datum and resolution. Preference in overlapping scenes is given to those with the least cloud or haze, and closest to late summer 1999. Imagery used is

[4] Checking for errors on a mosaicked DEM would be a project in itself, however it is possible that the total area of edge effects would be small enough to ignore.

summarized in table 4.2.2.

Landsat scenes used			
Row	Scene	Year	Month
56	16	2001	08
56	18	2000	06
57	16	1999	08
57	17	1999	08
58	18	2000	06
59	15	1999	08
59	16	1999	07
59	17	1999	08
61	15	1999	07
61	16	2001	06
61	17	2001	07

Table 4.2: Landsat scenes used to produce the regional mosaic image.

4.2.3 Field networks

Environment Yukon maintains a snow measurement network and issues a snow survey bulletin three times annually - after March 1, April 1 and May 1. Fifty-six locations are monitored for SD and SWE. A large historic record exists for this data set, with 5–48 years on record (Janowicz, 2008). This data set will be used to test the modelled algorithm for SD on an independent set.

Variable	abbreviation	units	source
Elevation	elev	meters	90 m DEM
Elevation range	elev_rng	meters	90 m DEM
Elevation standard deviation	elev_std_dev	meters	90 m DEM
Slope	slope	radians	90 m DEM
Aspect	aspect_sin, aspect_cos; aspect_fac	sine&cosine(radians); unitless	90 m DEM
Curvature: vertical, horizontal	vcurv, hcurv	radians/meter	90 m DEM
Incoming radiation	solrad	Watt hours/m^2	90 m DEM
Position	lat, lon; x, y	decimal °, decimal °; meters, meters	90 m DEM
NDVI	ndvi	digital number	landsat 7 imagery
Tasseled cap: bright, green, wet	ts_bright, ts_green, ts_wet	unitless	landsat 7 imagery
Supervised classification	lc_sat	unitless	landsat 7 imagery

Table 4.3: Summary of variables, units, and data source.

4.3 Data collection

4.3.1 Stratified hierarchical sampling design

To achieve the goal of a wide area map of SD or SWE, the sampling strategy must be one that encompasses a large area. Logistical limitations prohibit intensive sampling over the whole area, so a subset was chosen close to winter roads. Sites were chosen within a stratification of driving distance from base camps.

Watson et al. (2006) showed that a stratified sample gave more efficient estimates of model parameters than a simple random sample given the constraints associated with acquiring measurements of SD and SWE (Elder et al. (1991) also suggests a stratified random sample, as the basis of an optimal sampling design, with stratifications based on terrain and radiation parameters.). From this work and its implementation in Watson et al. (2006), Jost et al. (2007) and Winkler et al. (2005) perform a simplified version, achieving similar performance.

A simplified version of this was implemented in this work. Watson et al. (2006) also make a number of observations on the inadequacy of typical sampling procedures. They suggest that due to spatial autocorrelation, the *in-situ* snow variation reported by many studies is biased downwards, as sample locations are closely spaced. Multiple sampling at short range allows for larger than point support, and thus more comparability to model data, which will likely have areal support from included DEM data. Mixed-effects models furthermore allow us to estimate variance components corresponding to different levels of the sampling design, and thus different spatial scales.

The sampling design in this study consisted of four hierarchical levels: year, transect, site, and measurement, and covered different topographic and landcover units through

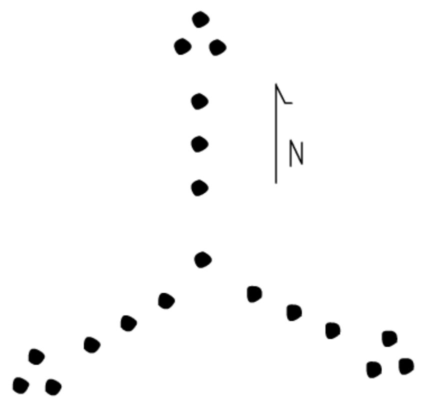

(a) Site design

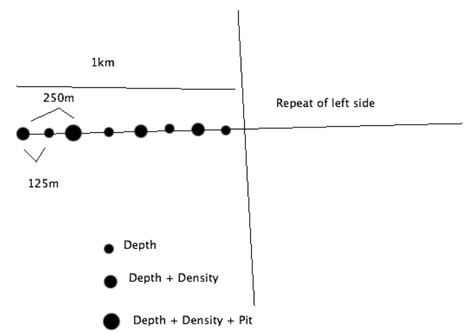

(b) Transect design

Figure 4.2: Sample design for the fieldwork. A number of (a) sites are nested within each (b) transect.

stratified transect selection. Through GIS analysis, the accessible portion of the study area was stratified based on terrain attributes. Then a set of locations for transects were randomly selected from these stratifications.

For each transect location, a traversable location was chosen in its vicinity (subject to property and terrain accessibility), and a transect was walked from this point. Each transect (Figure 4.2b) was made up of a number of intensive study sites arranged in a line, separated by 125 m, as measured from center-point to center-point. This distance was chosen so that the distance between measurement sites would be 100m, when SD measurements could be considered to be independent in a similar land cover (Pomeroy & Gray, 1995).

Each intensive study site (Figure 4.3.1) was laid out as an equilateral triangle, with a distance from the center to a vertex of 16m. At each vertex 3 SD samples were taken in a 1 m equilateral triangle. From the vertex back to the center an additional 4 equally spaced measurements were taken, as described by Watson et al. (2006), modified by adding

Comparison of field data to study area averages

variable	median.field	IQR.field	median.area	IQR.area
elev	706.00	251.00	1030.00	496.00
slope	0.04	0.11	0.16	0.22
hcurv	0.00	0.00	0.00	0.00
vcurv	-0.00	0.00	-0.00	0.00
elev_stdev	7.76	13.88	22.57	27.27
elev_rng	32.00	50.00	84.00	101.00
ndvi	187.00	73.00	202.00	50.00
ts_bright	115.00	56.00	106.00	52.00
ts_green	187.00	53.00	200.00	34.00
ts_wet	137.00	65.00	146.00	63.00
solrad	136203.52	8495.00	74123.92	15990.64
aspect_sin	-0.18	1.50	-0.04	1.48
aspect_cos	0.24	1.32	0.07	1.34

Table 4.4: Comparison of field sites and study area terrain attributes. Distributions are non-normal therefore median and interquartile range are reported.

measurements along the lines from center to vertex. This alteration was done to facilitate rapid movement through difficult terrain. The goal of the measurement design was to construct a within-site variogram representing the spatial autocorrelation of measurements.

At the center of every other sample site, a measurement of SWE was taken either by snow pit, or density core (ESC-30 snow tube). One pit was dug per transect, and the remainder were density measurements. These allow the SD measurements to be converted to SWE measurements, as density was expected to change conservatively over space as compared with SD (Elder et al., 1998).

Overall, 37 transects with 214 sites were visited in the field (Figure reffig:sampleLocations) in the two years of the study, containing a total of 7869 observations of SD, and 361 observations of snow density.

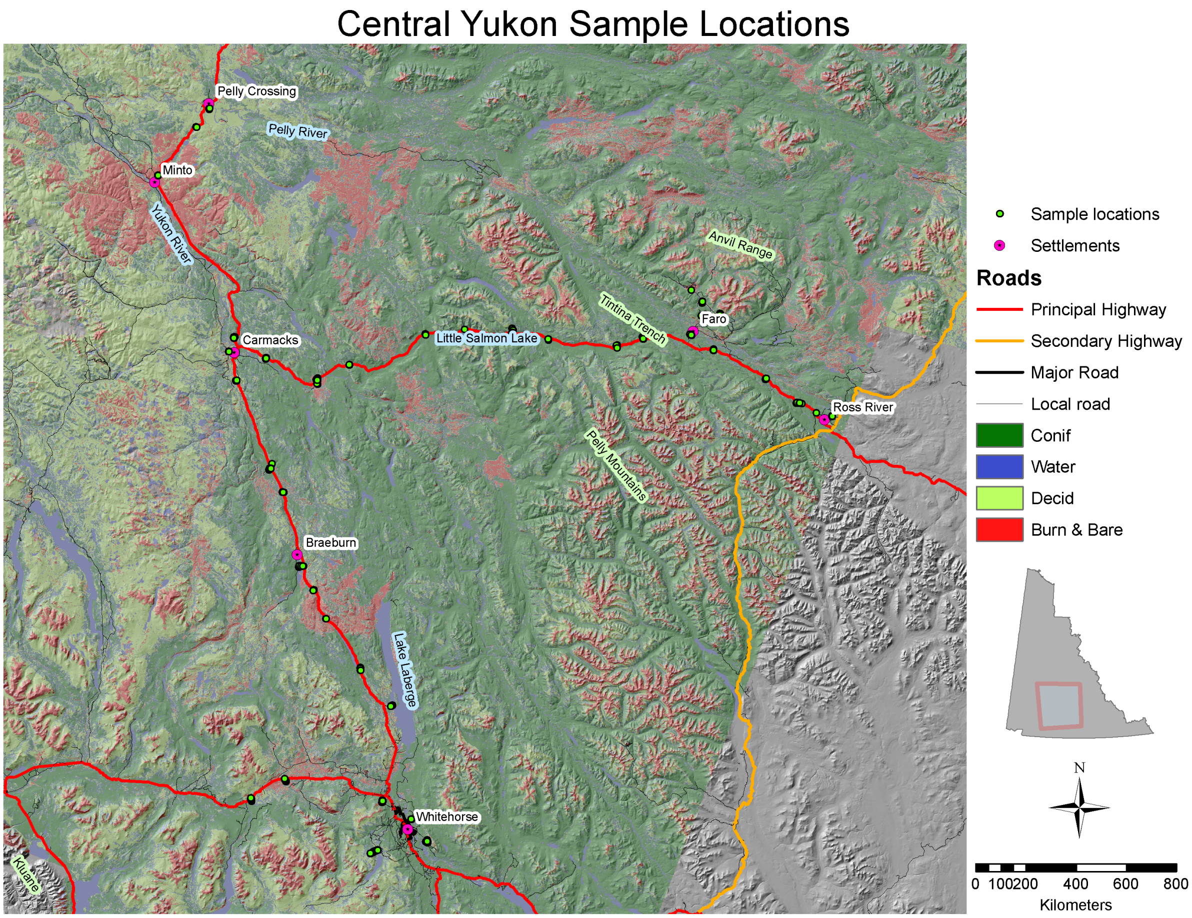

Figure 4.3: Locations of field samples (green circles) for 2008 and 2009.

4.3.2 Sampling methods

Snow depth measurement: SD was measured with the Magna-Probe. Depth measurements are accurate to a few mm (Magnaprobe manual). Depths were taken parallel to gravity, as per Cline et al. (2001), and the CLPX experiment (Elder et al., 2009). Measurements were located by hand-held GPS , and were taken as precisely as possible, including in tree-wells, so as to reduce selection bias. If the probe struck rock or wood before ground, a new point was taken as close as possible. Care was taken to have the probe basket rest on top of the snow surface, but with extremely fluffy or fresh snow it might sink in up to 1 cm. Each point was georeferenced referenced with the integral GPS unit.

Snow density measurement: Snow density was sampled with an ESC-30 snow corer. Three measurements were taken in an equilateral triangle of edge length 1 m located at the center of a study site. Cored snow was measured on a spring scale. Some inaccuracy was accrued during warmer periods of the day as snow would adhere to the inside of the tube. Snow depths for this measurement are read to the nearest 0.5 cm on a 1 cm scale. Spring scale measurement was to nearest 5 g for large amounts, or nearest 1 g for smaller amounts.

Snow pit measurements: Once per transect a snow pit was dug. Snow stratigraphy was subjectively determined based on changes in snow grain size, ice layers, crystal form, and snowpack strength. Snow density was measured by density cutter, 1 L for the larger and 100 ml for the smaller. One density profile was cut, using the larger cutter when possible (10 cm chapters), and the small cutter when necessary to complete a layer (2.5 cm chapters). Vegetation, depth hoar, and air pockets limit the accuracy of the last measurements closest to the ground. Temperature was measured for: air, and once per layer with a thermometer to the nearest degree. In the second sampling year, basal temperature at the snow/ground interface was also measured. Grain size was measured in each layer with a 10x lens and 1 mm grid. The same spring scale as for density measurements was used.

4.3.3 Transect identification

4.3.4 Data preparation

- Snow depth data: From the fieldwork dataset, we first eliminate all points not in the survey class of 'site', this removes the extra along-transect measures. We then eliminate points where a mistake was made in taking the measurement (as recorded by the magnaprobe operator in the field). Points on which the magnaprobe wrote bad information to memory were also removed (22 points). GPS coordinates were corrected as per the Magnaprobe manual, but could not be differentially corrected due to lack of full satellite records. Positional precision is 0.0108 arc seconds, whereas accuracy was dependant on satellite constellation and interfering vegetation and obstacles. Handheld GPS reported an accuracy of 3–10 m.

During the second field season, the Magnaprobe operator display was damaged, prohibiting display of calibration tests, and record numbering. Sites were and error readings were delimitated by a sequence of min/max readings. These were removed and properly labelled during data preparation.

- Snow pit data: Pit data was manually entered into the computer from field books during and after the field season. GPS coordinates were assigned to each site from the SD data.

- Auxiliary information: Information from the DEM and landsat imagery were then added to the field data set using the corrected GPS co-ordinates.

4.4 Mixed effects regression procedure

As the data set was multi-level, and its measurements were correlated within the hierarchy, the MER model was used, as described by Pinheiro & Bates (2000); who suggest a model building strategy that first builds a no-fixed effects model with the random effects specified. Then, in a forward-stepwise manner, candidate fixed effects were added and tested for significance using the t-test. The next candidate fixed effect was chosen by graphical interpretation of structure in a plot of estimated random effects versus covariate. Included random effects were be dropped if a fixed effect accounts for the intergroup variation.

4.4.1 Random effects

The random effects were then defined: year (as López-Moreno & Stähli (2008)), transect, and site for the variables to describe the nesting structure, and thus describe the random sample of the population. The direct contribution of transect or site on SD was not required, but rather the effect of the structure on the model fitting was needed to allow for the non-independence of samples. With a more extensive field set, additional effects could also be described as both random and fixed, such as elevation or landcover. However, without enough samples, this would reduce the ability of the fitting algorithms to find a solution. The random effects were configured to only adjust the intercept, not slope for the different locations. This was the simplest formulation. The hierarchy of random effects was defined as measurements nested within sites, nested within transects, nested within years. This controlled how parameters were estimated from observations, ensuring the estimation adhered to the sampling strategy.

A parsimonious model was desired, such that as many candidates for fixed effects as possible could be discarded. Optimally those fixed effects that were highly correlated with other fixed effects, or which contributed the least to the model fit will be discarded. The list of independent variables includes the transformed and centered variables as well as the untransformed variables so as to test the value of the transformation.

4.4.2 Fixed effects

The fixed effects procedure followed a number of distinct steps. These steps allowed the selection and adjustment of a subset of potential variables, and corrections for the assumptions of the chosen model.

1. Regressor selection: Stepwise selection was the tool best suited to reducing a large number of possible regressors because it ensures impartial selection of terms included in the model space. In accordance with Pinheiro & Bates (2000), a forward stepwise search was conducted. Rather than the suggested visual inspection of candidate regressors plotted against random effects, a quantitative statistic was generated and compared. This allowed for bias free comparison, as well as allowing more of the parameter space to be explored. Pinheiro & Bates (2000) recommend against using log likelihood tests and ANOVA to compare models differing in fixed effects, as the statistics will be unpredictably under or over conservative. Although an adjustment method is described, an alternate statistic of goodness-of-fit was considered simpler. The statistic used was the sum of the standard deviations of all of the random effects. A reduction in this value indicates that the model explains more of the variance. Candidate regressors included all terms, as well as their listed transformations, in addition, a term representing the interaction of elevation and water was included.

   By using the above selection procedure, it was expected the following effects will occur: reported p-values for selected terms will be inflated, and p-values (if used further) must be assessed under the framework of multiple testing. These effects, and others, are standard to the use of term-reducing selection procedures (Faraway, 2006). In addition, predictor variables added towards the end of the selection might only represent noise in the sample, and thus harm the transferability of the final model (Harrell Jr. et al., 1984).

Stepwise selection was performed inside a transect-level cross-validation (CV) framework, as follows: for each transect the model was built up in a forward stepwise manner from the null model (random effects and intercept only) with that one transect excluded. The results of all leave-one-transect out CV are then pooled, and the final model formulation (Table 5.2) was chosen as all terms which were included in at least 50% of the cross-validation runs (Formula 5.1). This helps adjust for model shrinkage.

Furthermore, after the stepwise selection, the included terms in the CV-selected model which had a p-value greater than 0.50[5] in a marginal F-test were discarded, as are terms which are strongly correlated with other included terms. This p-value threshold was not considered as an overall measure of significance for term inclusion in the reduced model because multiple-testing has occurred, however, within the current model it may be used to compare the significance of the fixed effects.

2. Weighting: The MER model was designed to have a weights term added, where appropriate, to adjust for the within-group heteroscedasticity structure. The standardized residuals were plotted against fitted values and the included regression variables. For each of these possibilities for weighting an adjusted model was fit, and the resulting residuals were plotted again and assessed graphically (Figure 5.6, and 5.4), the best of these adjustment terms will be used in the final model.

3. Correlation structure: The model could have a within-group correlation structure specified, when appropriate to the data structure. This structure accounts for the

[5]This value of point-five is intentionally very large to cut out only the weakest terms. Adjusting p-values for multiple testing and using this value as a rule for inclusion/exclusion is too harsh.

spatial autocorrelation (SAC) of the measurements made within a site, and the sites within a transect. The within-site SAC were modelled using a variogram (Figure 5.3). The correlation, if any is found in this figure, will be used to fit the final model.

4. Final model: Finally, the variance adjustments and SAC corrections were combined and the model refit, using the model designed above, under restricted maximum likelihood (REML) estimator. This ensured that the model was not overly optimistic[6] about the variance and error terms.

4.5 Summary

- Variables: Elevation, the range and standard devation of elevation in a 270 m radius, the sine and cosine transformations of aspect, incoming solar radiation, NDVI and tasseled cap transformations of landsat imagery were used as potential predictor variables. Landsat data came from the years 1999–2001, acquired in the late summer, with low to no cloud cover. Elevation data came from Geomatics Yukon (B.2), processed in SAGA GIS (See appendix B.1).

- Data collection: Fieldwork was conducted in late March, early April of 2008 and 2009, during a two week intensive campaign. Observations were collected at sites contained within transects. This structure allowed for repeat observations with the minimum amount of time lost to transportation, while capturing the spatial variability of the observed quantities at several scales.

[6]REML estimation takes into account the loss of degrees of freedom to the estimation of the fixed effects, thus allowing fewer degrees of freedom to the residuals, and inflating the variance estimates. The estimations of ML and REML will converge, asymptotically with the number of observations. REML is applied in the final model refit, as the REML estimation procedure produces results which do not allow for log-likelihood comparisons between models with the same random effects structure.

- MER model building: A MER model was built, within a cross-validation framework to ensure the minimum amount of overfitting or shrinkage. The model was adjusted with weighting and correlation parameters to increase its robustness, and to mitigate violations of the MER assumptions. The final model was refit under REML to enhance the estimation of the random effects parameters.

Chapter 5

Results

5.1 Fieldwork results

Essential information on snow distributions in the central Yukon was gained from examining the raw field data. The coefficient of variation (CoV) has been presented in several papers as a useful measure of how variable a snow distribution is, generally by terrain unit. In figure 5.1 the CoVs are shown by land unit and year. Pomeroy & Gray (1995) listed the following CoV's of SWE: level plains: fallow (0.45), stubble (0.35); steep hills: pasture (0.55), brush (0.45). Using SD instead of SWE increases the CoV, because SD varies more than SWE over shorter distances. However, the basic breakdown of CoV should be similar between SD and SWE, wherein vegetation reduces and terrain slope increases the CoV (slope is strongly positively correlated with elevation in the study area) . This is evident in figure 5.1.

Examining the field work data by land cover class (Table 5.1), it is noted that the coefficient of variation (CV) for all land cover classes is approximately equal (in the all-years grouping), in contrast to the mean values, which show separability for most classes.

In 2008, and to a lesser extent 2009, when considered separately there was much more variability in snow depth and between classes.

Snow by landcover and year

Year	Group	Landcover	Min.	1st Qu.	Median	Mean	3rd Qu.	Max.	stdev	CV
08 & 09	Snow Depth	burn	0.792	29.3	48.7	47.7	61.9	120	19.552	0.41
08 & 09		water	11.6	20.8	31.6	30.1	36.4	53.5	10.068	0.334
08 & 09		coniferous	0.112	44.9	52.5	58.6	68.1	199	22.187	0.379
08 & 09		decidious	0.106	34.6	53.9	53.7	66.4	121	20.951	0.39
08 & 09	Density	burn	0.1	0.138	0.159	0.167	0.191	0.257	0.039	0.234
08 & 09		water	0.147	0.172	0.19	0.206	0.235	0.353	0.049	0.239
08 & 09		coniferous	0.084	0.149	0.178	0.182	0.202	0.357	0.044	0.244
08 & 09		decidious	0.075	0.155	0.178	0.18	0.201	0.31	0.041	0.228
2008	Snow Depth	burn	4.68	24	33.9	36.4	46.2	91.8	15.927	0.438
2008		water	11.6	16.6	20.1	23.1	28.8	41.2	8.629	0.374
2008		coniferous	0.112	43.1	48.9	51.5	55.8	121	15.804	0.307
2008		decidious	4.01	31.9	41.6	44.5	52.9	121	17.285	0.388
2008	Density	burn	0.1	0.137	0.154	0.163	0.189	0.257	0.04	0.243
2008		water	0.148	0.167	0.19	0.189	0.212	0.24	0.03	0.159
2008		coniferous	0.093	0.151	0.181	0.182	0.2	0.313	0.04	0.222
2008		decidious	0.075	0.155	0.172	0.174	0.194	0.267	0.043	0.25
2009	Snow Depth	burn	0.792	54.1	61.7	62.2	69.2	120	13.172	0.212
2009		water	14.8	29.9	33.9	34.4	37.6	53.5	8.32	0.242
2009		coniferous	0.22	59	70	74.4	88.1	199	25.995	0.349
2009		decidious	0.106	60	66.1	66.4	73.9	118	18.811	0.283
2009	Density	burn	0.105	0.147	0.164	0.171	0.192	0.242	0.039	0.225
2009		water	0.147	0.177	0.191	0.215	0.24	0.353	0.055	0.256
2009		coniferous	0.084	0.145	0.172	0.181	0.212	0.357	0.053	0.293
2009		decidious	0.121	0.164	0.182	0.186	0.204	0.31	0.038	0.202

Table 5.1: Summary of SD (cm) and density (g/cc) by land cover class

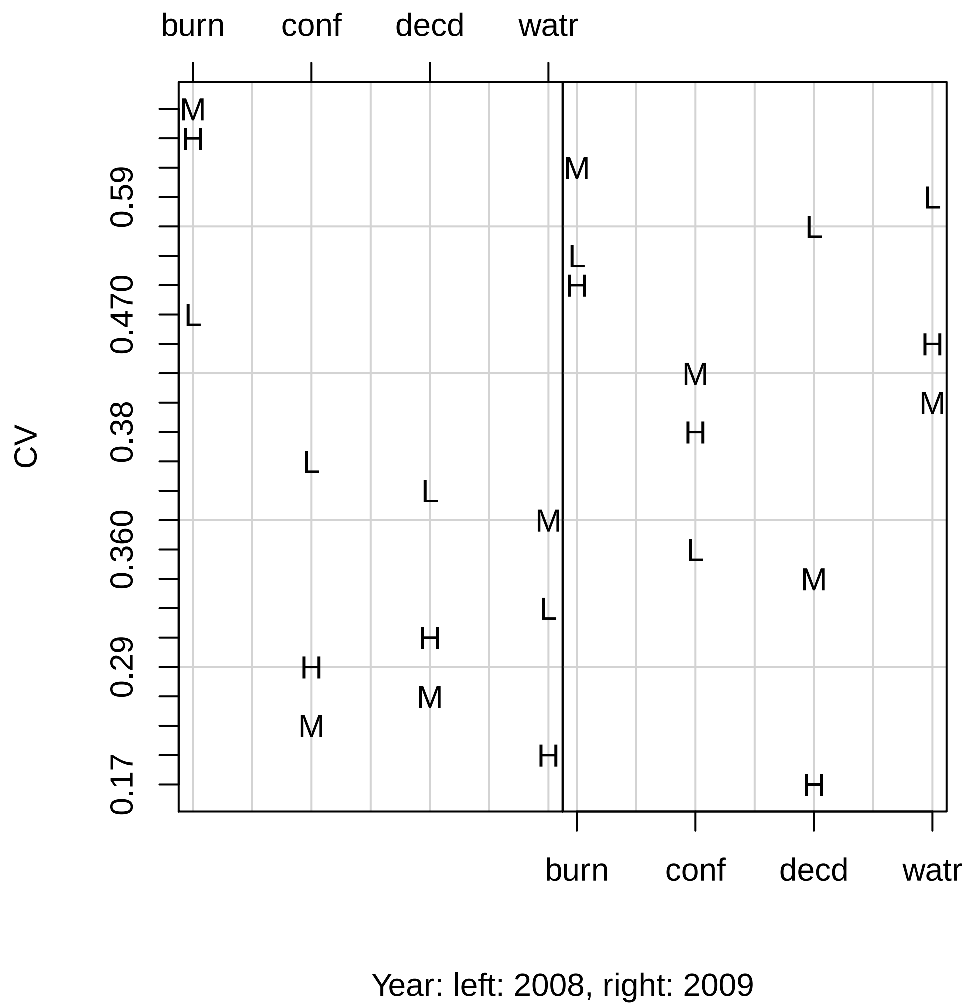

Figure 5.1: Coefficient of variation (standard deviation divided by the mean, used as a comparable measure of variation between different variables) for different land cover classes in both study years. Symbols indicate elevation: L: low, M: medium, H: high.

5.2 Fieldwork and design

By examining the values in table 4.4 and the first column of scatterplots in figure 5.5 the success of the transect location selection was assessed. In Elevation (elev), a bias to low elevations in sampling was present, since higher elevation sites were not accessible. This is further reflected in the slope, range, and stdev variables as these are correlated with elevation. The sampling of vegetation was satisfactory.

5.3 Analysis of field and ancillary data

Before the mixed-effects regression procedure was employed, an exploratory data analysis was undertaken to seek any key relationships in the data.

Fitting a binary regression tree on the data allows for the quick identification of inflections and interactions in the data set. Tree fitting is not necessarily globally optimal as the whole model space is not explored. Also no sub-set cross-validation was performed, so this technique is best used for quick exploration. Observing the tree (Figure 5.3), limited to 3 nodes deep, we see that elevation and landcover (via tassel cap and supervised classification) are chosen as the most significant breaks in the data set. This information can be used to cross-check the selection results of the stepwise MER process.

In figure 5.3 a within site scale SAC (bottom semivariogram) is visible having range of about 15m, accounting for about half of the semivariance, the rest being nugget. At the (within) transect scale (middle semivariogram) a sill was evident at the within-site scale of <30m, and it again occurred once enough distance has passed to include multiple whole sites (separated by 125m). At the whole transect scale (top semivariogram), a sill was very evident until about 1000 m where a scale-break was evident, probably due to the inclusion of multiple transects.

The general presence of a sill at approximately 25 meters, which holds steady until at least 500 m justifies the sampling procedure used. Intensive sampling below the range allows for characterization of the small-scale variability. The grouping in transects is logical, as there is a transect-level self-similarity.

Due to the alignment of the survey along highways, latitude and longitude are dropped as predictors, as they are too strongly correlated with elevation. This gives very poor coverage of the area, and so a potential trend of depth with location cannot be separated from the other attributes measured in each region. For instance, all of the very high elevation sites were in the NE of the study area, and were not representative of the study area's true elevation distribution, merely access. This would bias a relationship between position and depth, as measured SD at higher elevations was greater than at lower elevations (Figure 5.4).

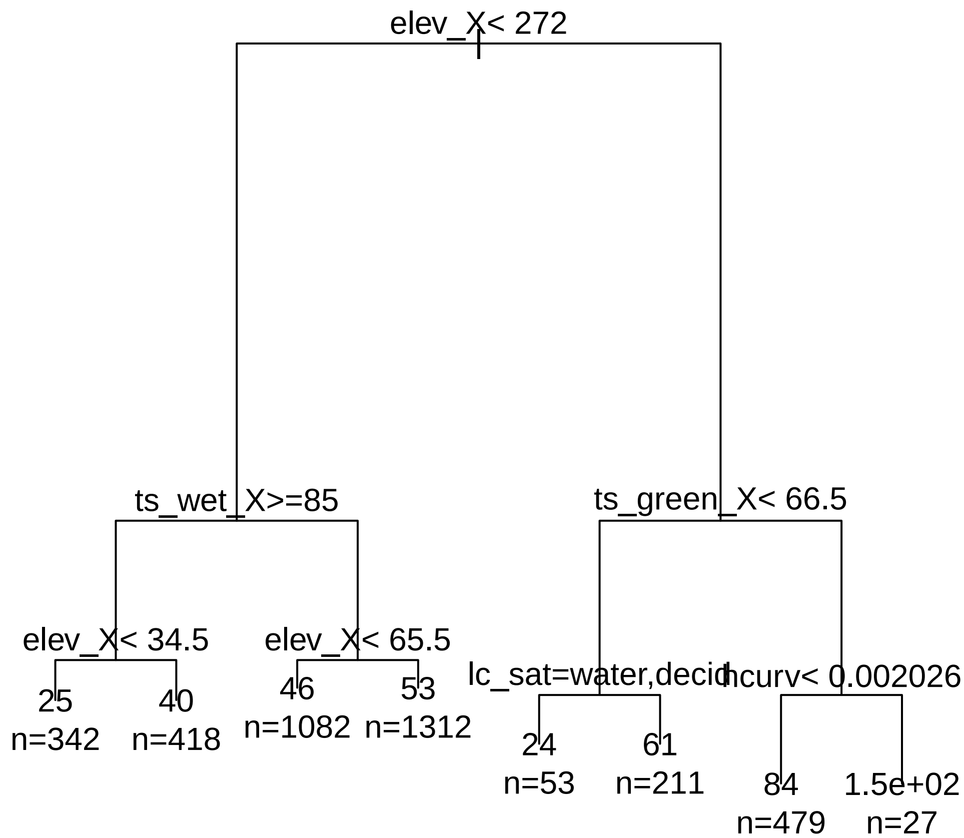

Figure 5.2: Simple binary regression tree, showing the partitionings which produce the most similar leaf nodes from the data set. Leaf nodes include counts of observations as well as the predicted SD(cm).

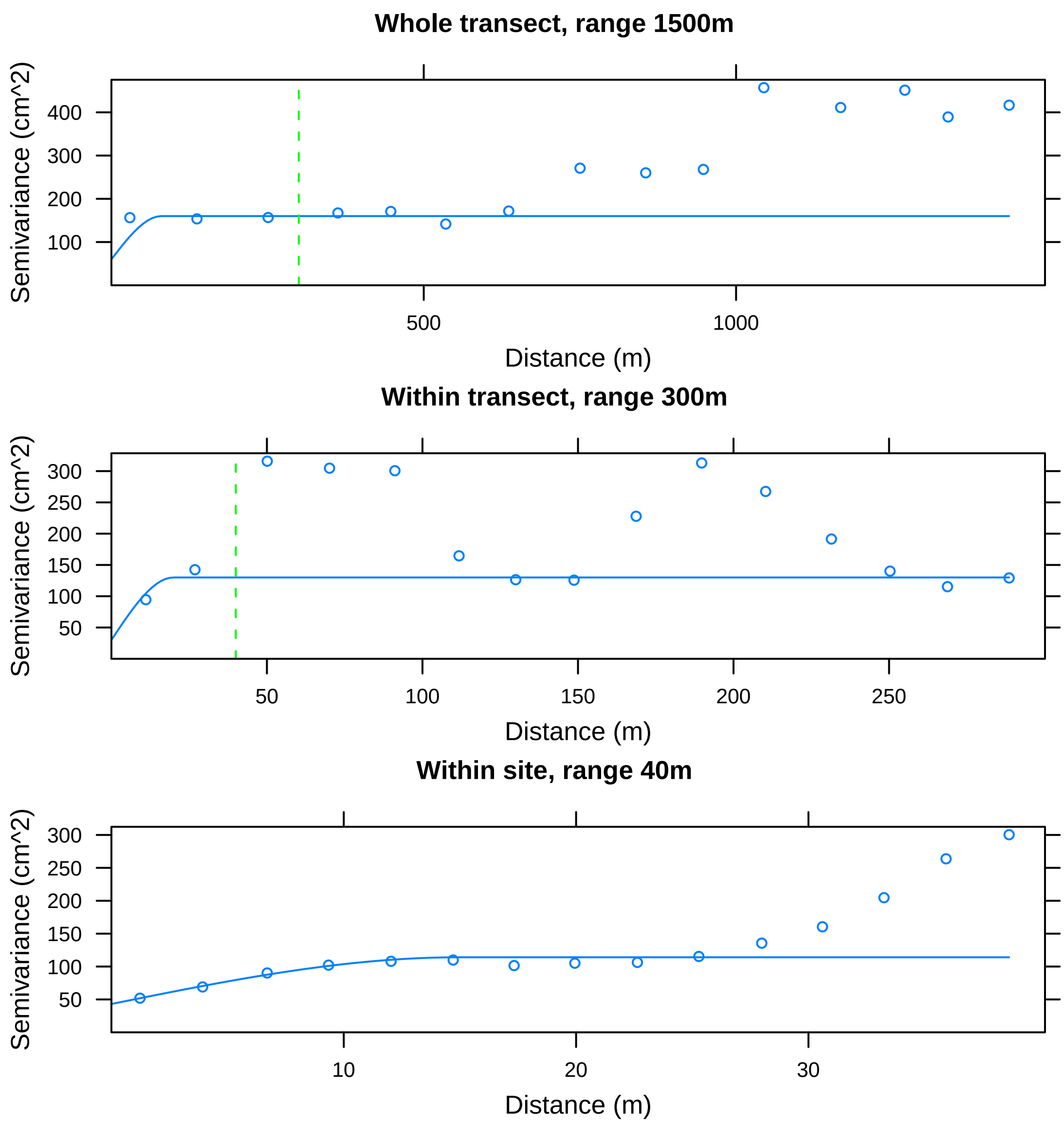

Figure 5.3: Residual semivariograms of SD at transect and site level. Semivariance is in cm^2. The dashed line in upper two figures shows the maximum lag distance of the figure below. A spherical variogram was fitted to each semivariogram.

A scatterplot of elevation and SD (Figures 5.5, 5.4) revealed a local minima in trend at 640 m a.s.l.. In addition, the response of elevation on water-covered surfaces was drastically different, presenting no strong trend. Above 1350m, the tree line in the field data, SD does not increase with elevation, likely due to wind redistribution. For this reason, a new variable (*isforest*) was created to categorize areas as water or above tree line, and its interaction with elevation.

In the landsat imagery there are a number of burn areas, all at least 9 years old (age of image). Any new burns since then will not appear in the model, and will count towards error in the landsat classification assessment. However, all post-burn forest regeneration should proceed at a locally-similar pace although it is acknowledged that local variability exists, which will reduce the impact on the study.

Scatterplots (figure 5.5) of predictor variables versus SD, grouped at the site level, were examined for non-linearities. A number of potential centerings to enhance the linear relationships were noted:

- Elevation (elev_X): center at 640.
- Slope, range, stdev (*_log): add $log(x + 1)$
- Aspect (aspect_(sin,cos)_X): center at 0
- All tassel (ts_*_X): center at 125
- Solrad (solrad_X): center at 136000.

An improvement in the linearity of the terms is evident in figure 5.5, especially the tasseled cap values. Non-linearity still exists in the remainder of the terms which cannot be removed by centering or simple transformations.

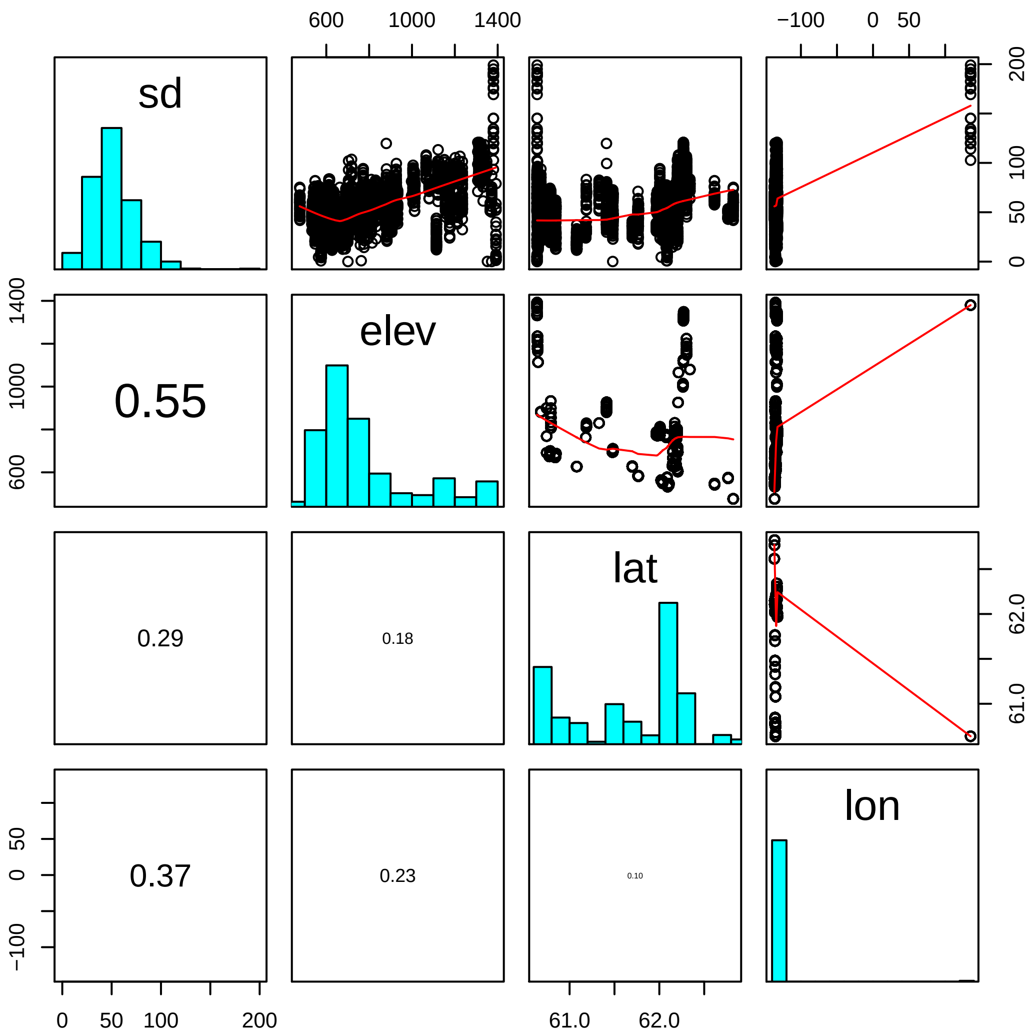

Figure 5.4: Bias for latitude and longitude. Numerical values in the lower left boxes are R^2correlation coefficients.

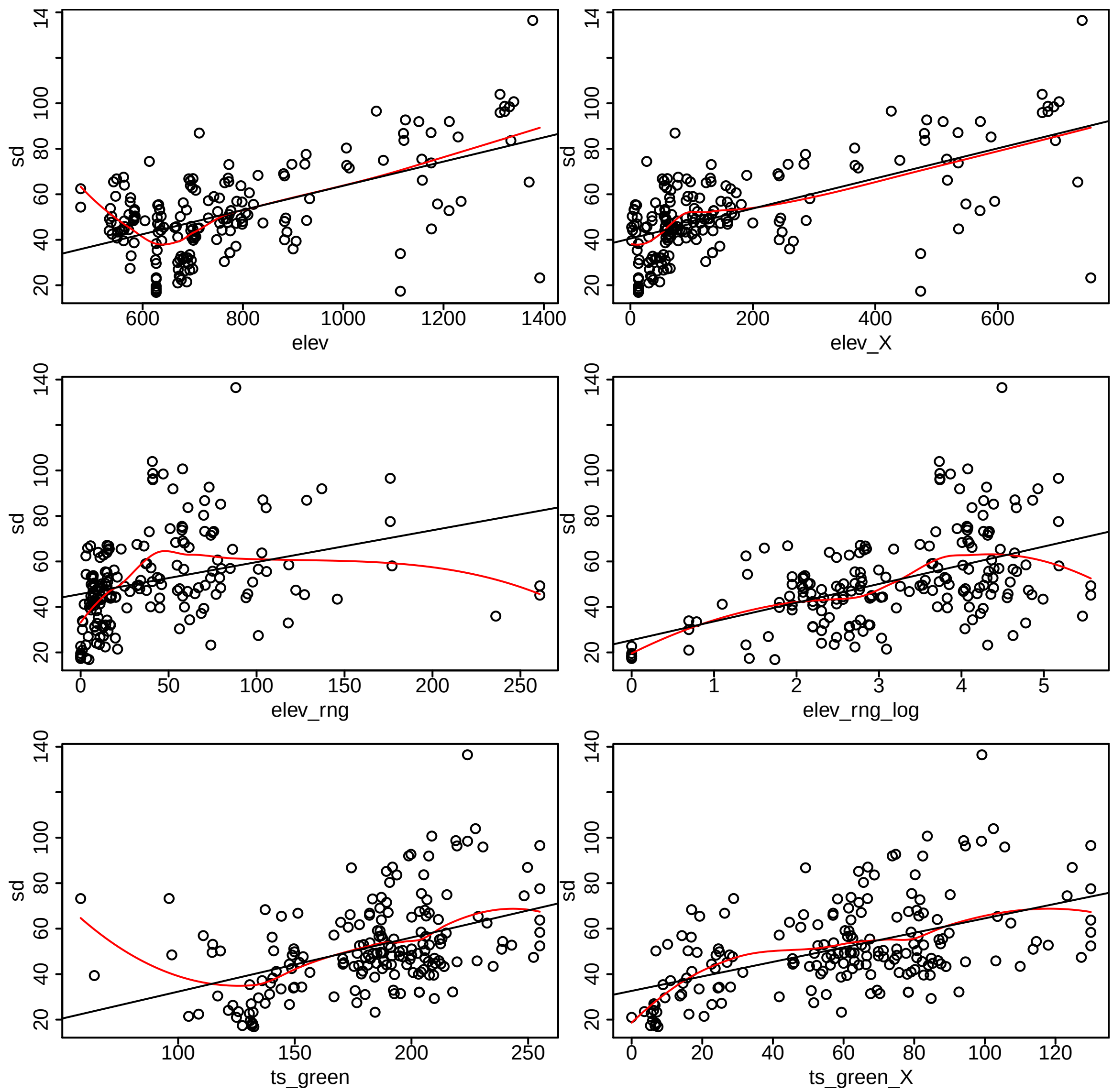

Figure 5.5: Transformations of select predictors (grouped at the site level, n=37), comparing observed (raw) data (left column) to transformed data (right column). The red line is a loess smoother fitting the data, and the black line represents a simple linear fit.

5.4 Model construction

- Stepwise selection

  Equation 5.2 contains the results of stepwise selection procedure to reduce the full model with all terms to a sub-model including only terms with a detectable and significant contribution. SD was calculated as the sum of the included terms multiplied by their respective regression coefficients. The symbol ":" indicates the interaction of the variable before and after.

$$\begin{aligned} sd \sim hcurv + aspect\_sin\_X + aspect\_cos\_X + elev\_rng\_log \\ +ts\_bright\_X + ts\_green\_X + elev\_X : isforest \end{aligned} \tag{5.1}$$

$$\begin{aligned} sd \sim hcurv + aspect\_cos\_X + elev\_rng_log + ts\_bright\_X \\ +ts\_green\_X + elev\_X : isforest \end{aligned} \tag{5.2}$$

Model terms by CV	
	% Included
elev	47.2
elev_X	0.0
slope	8.3
slope_log	8.3
hcurv	97.2
vcurv	2.8
hcurv_X	11.1
vcurv_X	0.0
aspect_sin	0.0
aspect_cos	0.0
solrad	0.0
aspect_sin_X	100.0
aspect_cos_X	22.2
solrad_X	0.0
elev_stdev	2.8
elev_stdev_log	0.0
elev_rng	2.8
elev_rng_log	97.2
ndvi	0.0
ts_bright	0.0
ts_green	0.0
ts_wet	0.0
ts_bright_X	100.0
ts_green_X	94.4
ts_wet_X	2.8
elev_lctree	0.0
elev_nlctree	0.0
elev_X_lctree	100.0
elev_X_nlctree	100.0

Table 5.2: Terms included in stepwise CV selection, as percent of models term was included in.

- Weighting terms: by observing the plots (figures 5.6, 5.4, and 5.8) a heteroscedastic[1] structure can be seen, with a characteristic wedge shape increasing from left to right. In the plots, L3 indicates residuals using all of the grouping structure information, the best possible model formulation using the random effects, and L1 indicates residuals taken knowing only the year, the minimum information which will always be known. L2 are not shown, but contain information from the transect level of grouping as well. This L2 information isn't useful, as we will not be predicting at the transect level. Having examined all candidate regressors (not shown), it was seen that lc_sat, ndvi, elev_rng, ts_green_X, and fitted values bear closer inspection.

  The classified landcover, and a power adjustment of fitted terms provide the best overall adjustment.

  The two ratings: fitted (L 1) and lc_sat were combined (Figure 5.9), and found to be better in terms of the residual versus fitted scatterplots. This result indicates that variance was significantly different in different land covers, and also increased with the fitted value, non-linearly.

[1]Heteroscedastic: having a non-constant variance. Homoscedasticity is an assumption of linear regression.

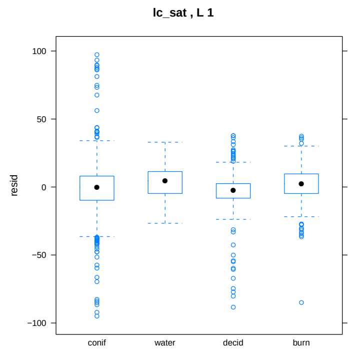

(a) Unadjusted land cover, year grouping level

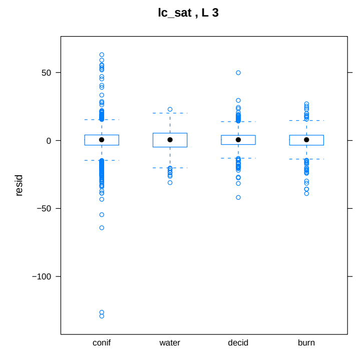

(b) Unadjusted land cover, all grouping levels

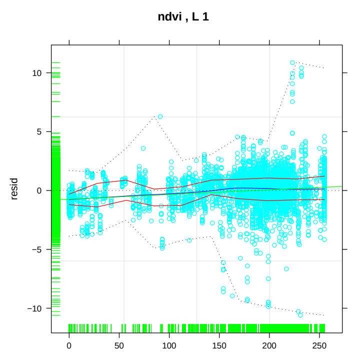

(c) Unadjusted NDVI, year grouping level

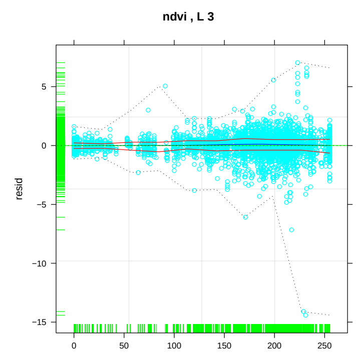

(d) Unadjusted NDVI, all grouping levels

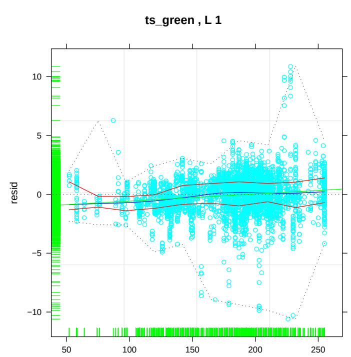

(e) Unadjusted ts_green, year grouping level

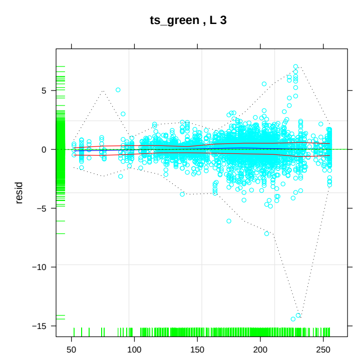

(f) Unadjusted ts_green, all grouping levels

Figure 5.6: Residual plots against variables: lc_sat, NDVI, and tassel greenness. All grouping information (L3) indicates residuals using all structural information, providing the best model formulation from random effects, and year only grouping information (L1) uses the minimum information which will always be known (the year).

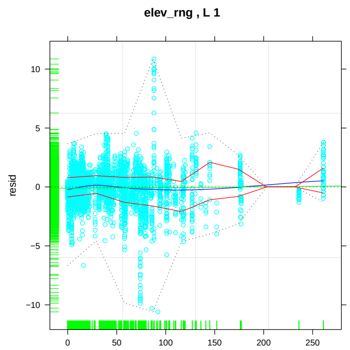

(a) Unadjusted elevation range, year grouping level

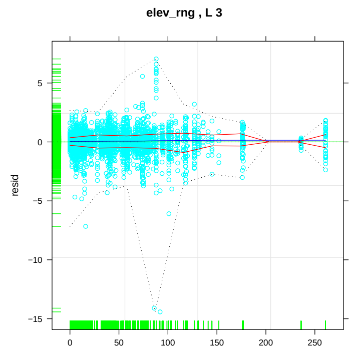

(b) Unadjusted elevation range, all grouping levels

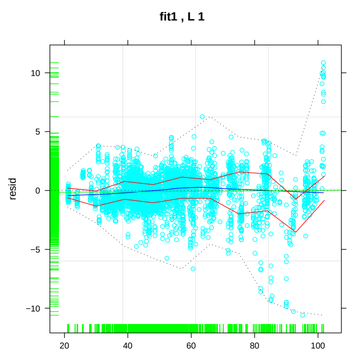

(c) Unadjusted fitted values (L1), year grouping level

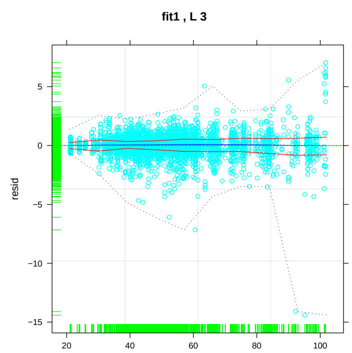

(d) Unadjusted fitted values (L1), all grouping levels

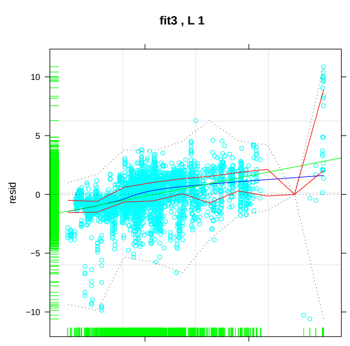

(e) Unadjusted fitted values (L3), year grouping level

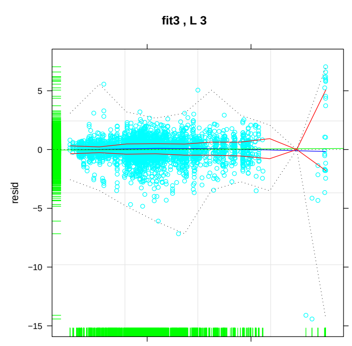

(f) Unadjusted fitted values (L3), all grouping levels

Figure 5.7: Figure 5.6, continued, weighting using elevation range, and fitted values (at both the L3 and L1 levels).

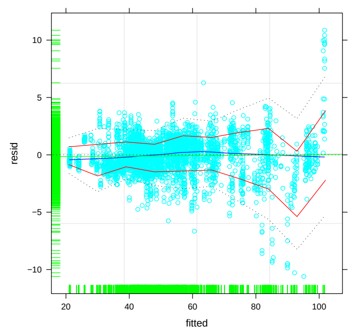

(a) Unadjusted model, L1

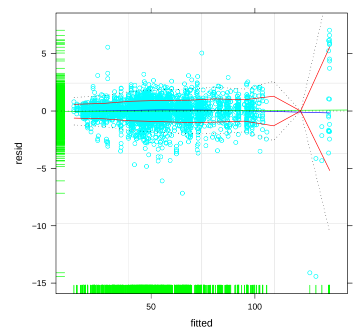

(b) Unadjusted model, L3

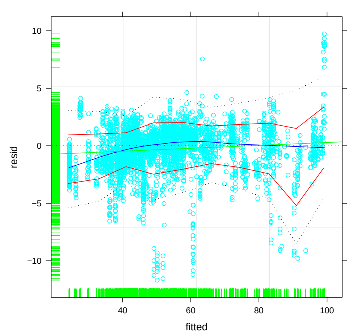

(c) Weighted by lc_sat, L1

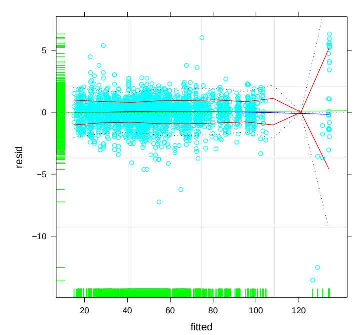

(d) Weighted by lc_sat, L3

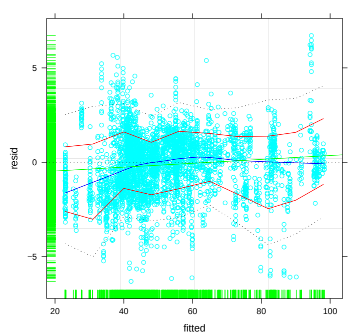

(e) Weighted by L1 fitted values, L1

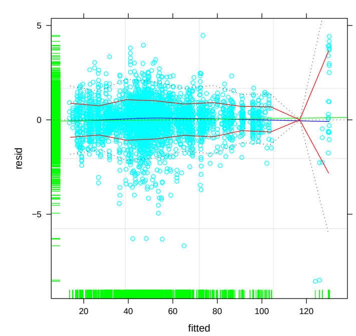

(f) Weighted by L1 fitted values, L3

Figure 5.8: Comparison of fitted vs residuals on 3 plots: unadjusted stepwise selection (repeated), weighted by fitted value, weighted by landcover class.

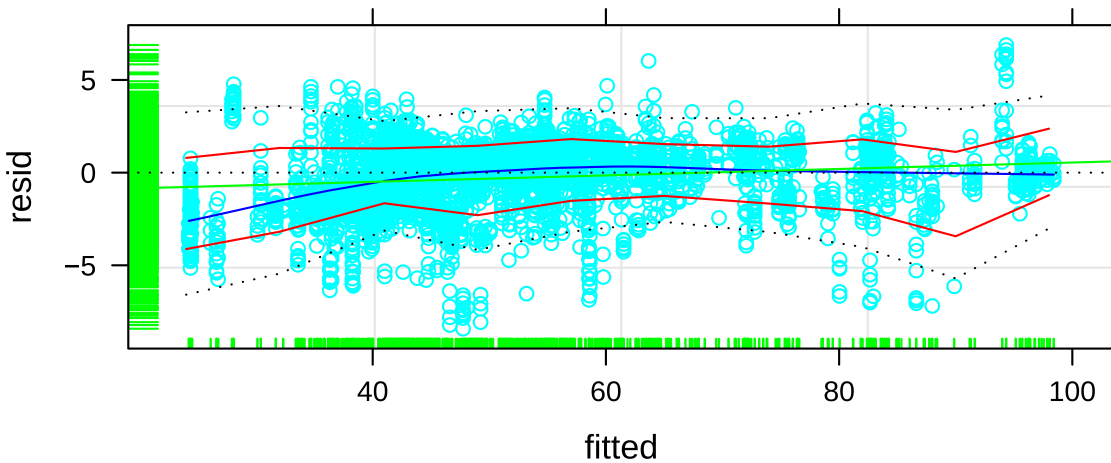

(a) Combined weighting with year only grouping

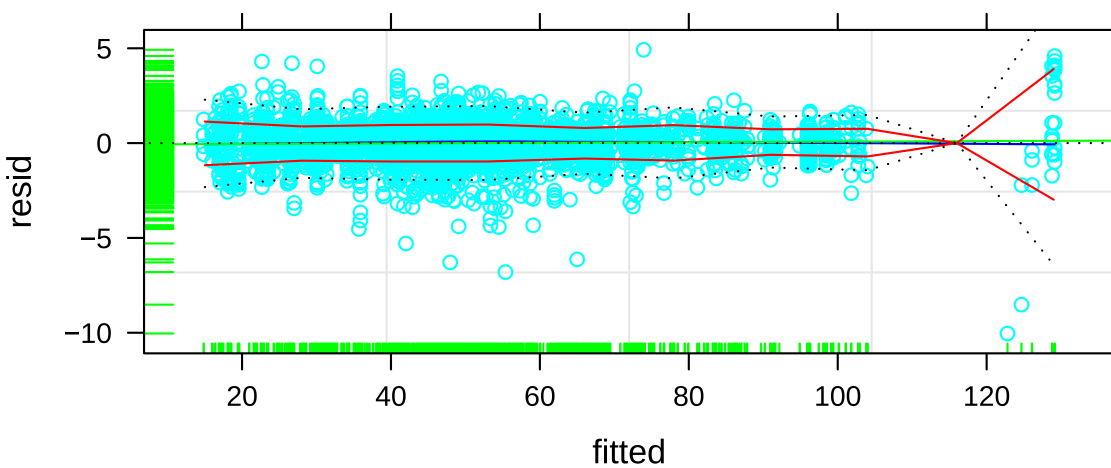

(b) Combined weighting with all grouping information

Figure 5.9: Residuals vs fitted values, weighted by the combination of L 1 (year only grouping) fitted values combined with separate variance by landcover classes. Figure (a) includes only the year for prediction, while (b) includes all available grouping information, which will not be available during final prediction.

- Correlation terms: examining the variograms in figure 5.3, the within site autocorrelation can be modelled with a spherical structure, with approximate values for range of 15 m, sill of 60 cm^2, and a nugget of 35 cm^2. At the transect and study region levels, the same basic spherical shape is evident, but is confused by the nested sampling design. At the transect level, the semivariance can be seen to rise suddenly at the transition between within site (<40 m), and the sampling lag distance between sites (40–125 m), as there were very few observations in these lag distance classes. When the next site along the transect is reached (125–155 m) the semivariance resumes its normal sill level, as it is now comparing two adjacent sites. This is the most probable explanation for the cyclic shape of the within transect residual semivariogram. The regional level (Whole transect) semivariogram has a scale break after 600 m. A possible explanation for this is that the majority of transects were only 500–1000 m long, so that semivariances in lag distances above might be due to the same phenomenon as in the within transect plot. It is also possible that a scale break exists at this lag distance, at which another distribution process becomes dominant.

  The model was adjusted for this site scale correlation structure, giving a value for the fitted spherical semivariogram model of: range 109.61, and a nugget factor (ratio of $nugget/sill$) of 0.184

5.5 Final model

The terms and parameters of the SD model are presented in table 5.3. The included terms have an understandable physical basis for interpretation. The inclusion of horizontal curvature implies a sheltering effect from wind, even without considering wind direction. Vertical curvature may be more sensitive to the wind direction, and is not included. Centered cosine of aspect relates to the east-westness of a slope, having potential implications for incoming radiation or wind shelter. Elevation range is an index of local terrain roughness, which may act to shelter pockets of snow from wind and sun. Tassel brightness indicates areas of bare ground, which are likely to be wind scoured. Tassel greenness indicates higher amounts of vegetation, which shelter and trap snow. SD increases with elevation *[NOTE: Derksen wants more details here, not sure what to add..]*(except when combined with lc_forest, i.e. above the tree line), and provides the largest contribution. This is a similar finding to many other regression studies.

Selecting the fixed effects terms using the above procedure, but for each year independently produces a similar selection of terms, but with an overall worse RMSE and total sum of standard deviations of fixed effects. The term selection in both cases produces a smaller subset of the two-year model, but the terms which are retained differ. Using the Bayesian information criterion (BIC), a penalized modification of the Akaike IC (AIC), as a selection criteria, despite the advice against produces the same fixed effects selection.

Final SD model

	term	value
Autocorrelation parameters	range (m)	70.000
	nugget	0.210
Weighting paramters	conif	1.000
	burn	0.810
	water	0.450
	decid	0.830
	power	0.660
Fixed effect coefficents	Intercept (cm)	40.000
	hcurv (rad/m)	1292.000
	aspect_cos_X (cos(degrees))	
	elev_rng_log (log(m))	1.200
	ts_bright_X (DN)	-0.098
	ts_green_X (DN)	0.073
	elev_X_lctree (m)	0.058
	elev_X_nlctree (cm)	0.017
Random effects coefficents	SDyear (cm)	8.701
	SDtransect (cm)	6.579
	SDsite (cm)	0.008
	SDres (cm)	1.111
Predictive performance	rmse_fit1	14.000
	rsq_fit1	0.780
	mbe1	-0.420

Table 5.3: Final model for snow depth (cm)

5.6 Model diagnostics

5.6.1 Cross-validation

The model was assessed by performing a leave-one (transect)-out spatial CV. No term selection was performed during this step, rather the range of values assigned to the included terms was scrutinized. Typical CV involves the systematic removal of a subset, random, or sequential. As the observations in this study are structurally pooled, the removal of a fixed number of observations would likely include multiple sites; and the removal of a single observation, as in standard leave-one-out CV would be ineffectual as there are at least 19 other nearby observations all highly autocorrelated. Therefore a spatial basis was used, so as to be strict and to respect the spatial groupings of the field data. This approach is similar to the spatial CV undertaken in Brenning et al. (2006), necessitated by the autocorrelation of neighbouring observations.

The transect level was chosen over the site level for CV as two sites within a transect are very likely to be so similar as to not give a large impact. In addition, the number of CV runs would then be much larger, and transect level already provides sufficient repeats. Table 5.4 contains a summary of the change in model statistics. The model was found to be reasonably stable, with the variation of the most influential terms below 10%, and the change in RMSE between fits having a coefficient of variation of 1%. The large range in the weighting parameter for SD variance for the water land cover class is likely due to the lack of sufficient CV runs, which in turn was caused by the lack of sufficient sampling sites at water sites. More water sites would either reduce the range of CV estimations or confirm the extremely variable nature.

Cross-validation of the final model

	term	mean	stdev	p_value
Autocorrelation parameters	range (m)	62.9147	19.6377	
	nugget	0.2233	0.0485	
Weighting paramters	conif	1.0000	0.0000	
	burn	0.8425	0.1711	
	water	0.4521	0.0203	
	decid	0.8614	0.1756	
	power	0.6716	0.0442	
Fixed effect coefficents	Intercept (cm)	40.2166	0.3867	0.0000
	hcurv (rad/m)	1359.4724	486.7871	0.0001
	aspect_sin_X (cos(degrees))	-1.2125	0.4206	0.3913
	elev_rng_log (log(m))	1.2363	0.1207	0.0608
	ts_bright_X (DN)	-0.0962	0.0056	0.0000
	ts_green_X (DN)	0.0724	0.0051	0.0003
	elev_X_lctree (m)	0.0576	0.0026	0.0000
	elev_X_nlctree (m)	0.0169	0.0042	0.0000
Predictive performance	rmse_fit1 (cm)	14.0925	0.4983	

Table 5.4: Cross-validation of the final model, no selection of fixed effects. RMSE_fit1 is the root mean squared error between observed and fitted values considered knowing(level of prediction) only the year.

5.6.2 External validation

The government of the Yukon maintains a number of snow courses in the province which are traversed three times per year. The April 1st transects coincide with this study. 17 of the transects are within the study area. The final SD model was used to predict a SD for these sites in both 2008 and 2009, and the results compared (Table 5.5) to the measured values. Predictions made for sites identified as water were very poor. When these were removed, R^2improved to 0.38 and 0.223 for 2008 and 2009. It is possible, that these transects were not correctly georeferenced to the Landsat imagery, and that they were not then actually in the water class. Forest identified sites also performed better than burn identified sites, possibly due to the combination of burn and bare classifications.

Prediction at snow bulletin sites		
Year	RMSE	Rsq
2008	29.015	0.220
2009	29.142	0.167

Table 5.5: Model predictions for Yukon snow bulletin sites.

5.6.3 Random effects structure

To demonstrate the utility of the random effects structure, the adjusted model was compared with a generalized least squares (GLS) regression model (Pinheiro & Bates, 2000) . The GLS model was constructed with the same weighting and correlation structure, but without any random effects. Examination of the GLS results (Table 5.6) demonstrate that the GLS model estimates are much larger in range and smaller nugget variance than the MER model. This was due to the MER model building an individual variogram for each site, and then combining. The GLS also does not estimate the variance components associated with the grouping structure, which, while not central to the results of this study, may be of interest[2]. The general form of the fixed effects in both the MER and GLS are similar in direction and magnitude, with the exception of *cos(aspect)*, being opposite in sign, and 1/3 magnitude, and *elev_rng_log* being four times larger. (NOTE: Claude wants to know why. I'm not sure this is entirely knowable.) It was therefore concluded that the MER model with random effects provided significant advantage, having both a decreased RMSE (16.0324028329959 at L3 (no L1 equivalent available) compared to 12.3846053577612 at L3 or 14.1163987873462 at L1), and a more plausible autocorrelation structure.

Examining the Quantile-Quantile (QQ) plot (Figure 5.10b) for the random effects struc-

[2] To those conducting further snow surveys, an understanding of the SAC of the SD and SWE fields is required to produce a sampling scheme that will both produce independent samples, and capture the local scale variation. The results and methods of this study can provide guidance in this area.

multicolumn4cComparison of MER and GLS models

	term	MER	GLS
Autocorrelation parameters	range (m)	70	154
	nugget	0.21	0.11
Weighting paramters	conif	1	1
	burn	0.81	0.82
	water	0.45	0.45
	decid	0.83	0.86
	power	0.66	0.47
Fixed effect coefficents	Intercept (cm)	40	28
	hcurv (rad/m)	1292	1464
	aspect_sin_X (cos(rad))	-1.1	0.12
	elev_rng_log log(m)	1.2	3.9
	ts_bright_X (DN)	-0.098	-0.054
	ts_green_X (DN)	0.073	0.078
	elev_X_lctree (m)	0.058	0.057
	elev_X_nlctree (m)	0.017	0.0077
Predictive performance	rmse_fit3 (cm)	12	16

Table 5.6: Comparison of final MER model and GLS model.

ture allows the assessment the distribution of the random effects. Ideally, the random effects should follow the normal distribution. Site level random effect of the intercept was normal, with very few outliers.

Since there was only one random effect estimated, the intercept, there are no correlations within the random effects to check for, and no further adjustment of the covariance matrix was required.

Second, the fixed effects component of the adjusted model was examined to ensure that the assumptions of the MER were met. The assumption of mean zero, constant variance in within-group errors are checked graphically in figure 5.10a. Errors (Pearson standardized residuals) are centered around 0, with the general heteroscedastic influences from fixed effects removed. Some amount of heteroscedacity still remains, however no relationships to any of the fixed or random effects was found, so no further weighting was appropriate. As a consequence of this result, the estimated standard error is likely to be inflated.

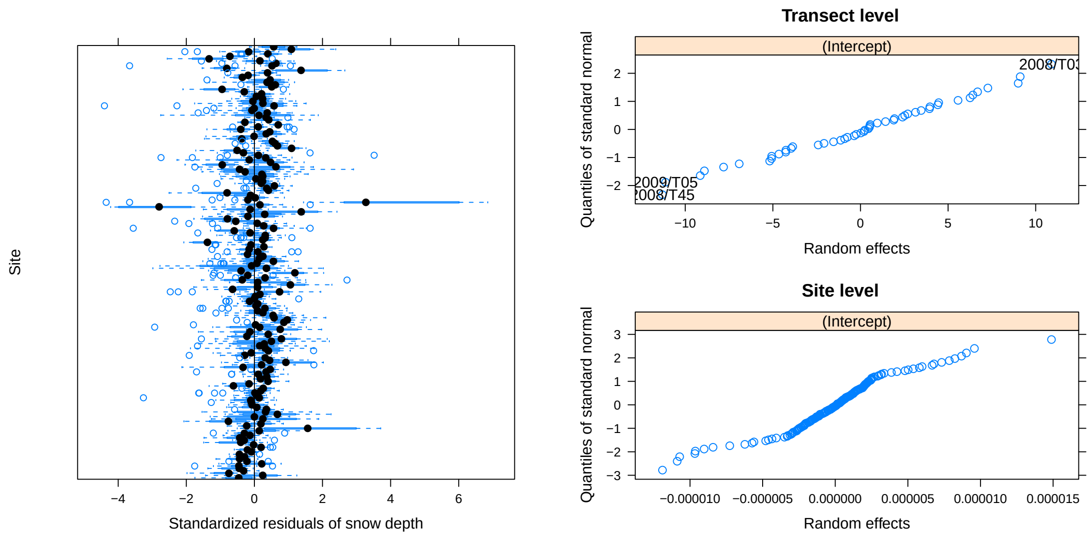

(a) (b)

Figure 5.10: (5.10a): Residuals vs fitted values boxplot. Mean values (residuals for SD) for each site are plotted as a solid dot, quartiles of values are plotted as box (50%), and whisker (75%), with outliers as empty dots. Assumptions of the MER model are mean of zero (indicated by the solid line), and constant variance (indicated by the width of the boxes).

(5.10b): Q-Q plot to assess normality of random effects at transect and site level. Potential outliers to the normal distribution are labeled. Plotted values are the differences in intercept for each site (marked as Year / Transect number / site number), from the overall average intercept (in cm). A mean zero and a normal distribution are expected. The y-axis shows the expected value if the distribution is normal. Therefore a straight line of points show that the distribution of random effects is approximately normal.

The assumption of normality of within-group errors was assessed graphically in figure 5.11.The adjustments to the model have improved the distribution towards normal, however the tails are still heavy. This may be due to SD being bounded by a minimum depth of zero, or by the minimum snow capture of even the smoothest sites (lakes). This departure from normality will inflate the standard error, and bias the F-tests for fixed effects. This is less of a concern as the model was chosen on its variance reducing capability rather than F-test for significance of fixed effects. Also, the modelling interaction terms between predictor variables has been avoided in this study for two reasons: first, the number of available data points was not sufficient to work with the vast number of possible co-linearities produced by even a second order interaction; and second, the SD values at higher elevations are achieved without field measurements and, therefore, limits the potential explanatory power of interaction terms (Jost et al., 2007).

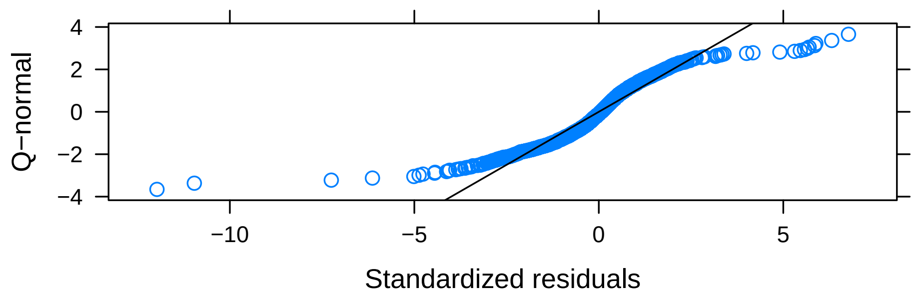

(a) Full stepwise model

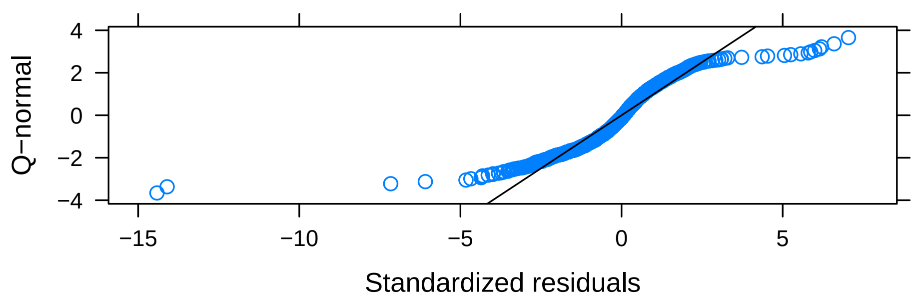

(b) Reduced stepwise model

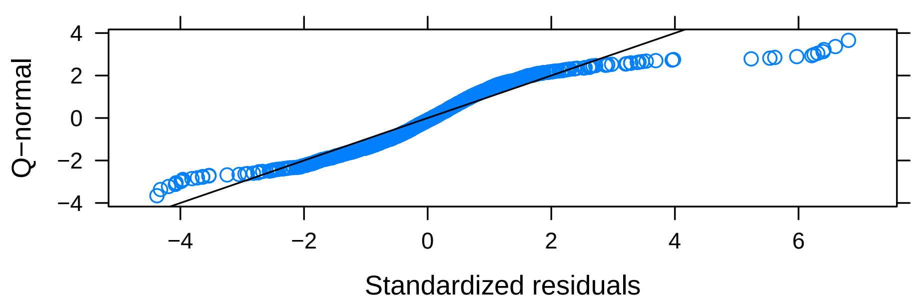

(c) Adjusted stepwise model

Figure 5.11: Q-Q plot to assess normality, full model vs adjusted and reduced model. Plot is of standardized residuals for fitted SD (open circles) plotted against their expected value (Quantiles of standard normal) if they follow the normal distribution. Points on or very near the solid line meet this assumption.

5.7 Map of snow depth

The predicted SD from the model is presented in figure 5.12. Areas in high mountains (right hand region of the map) were well outside the sampling range of elevation in the model and are thus highly uncertain, and should not be relied upon.

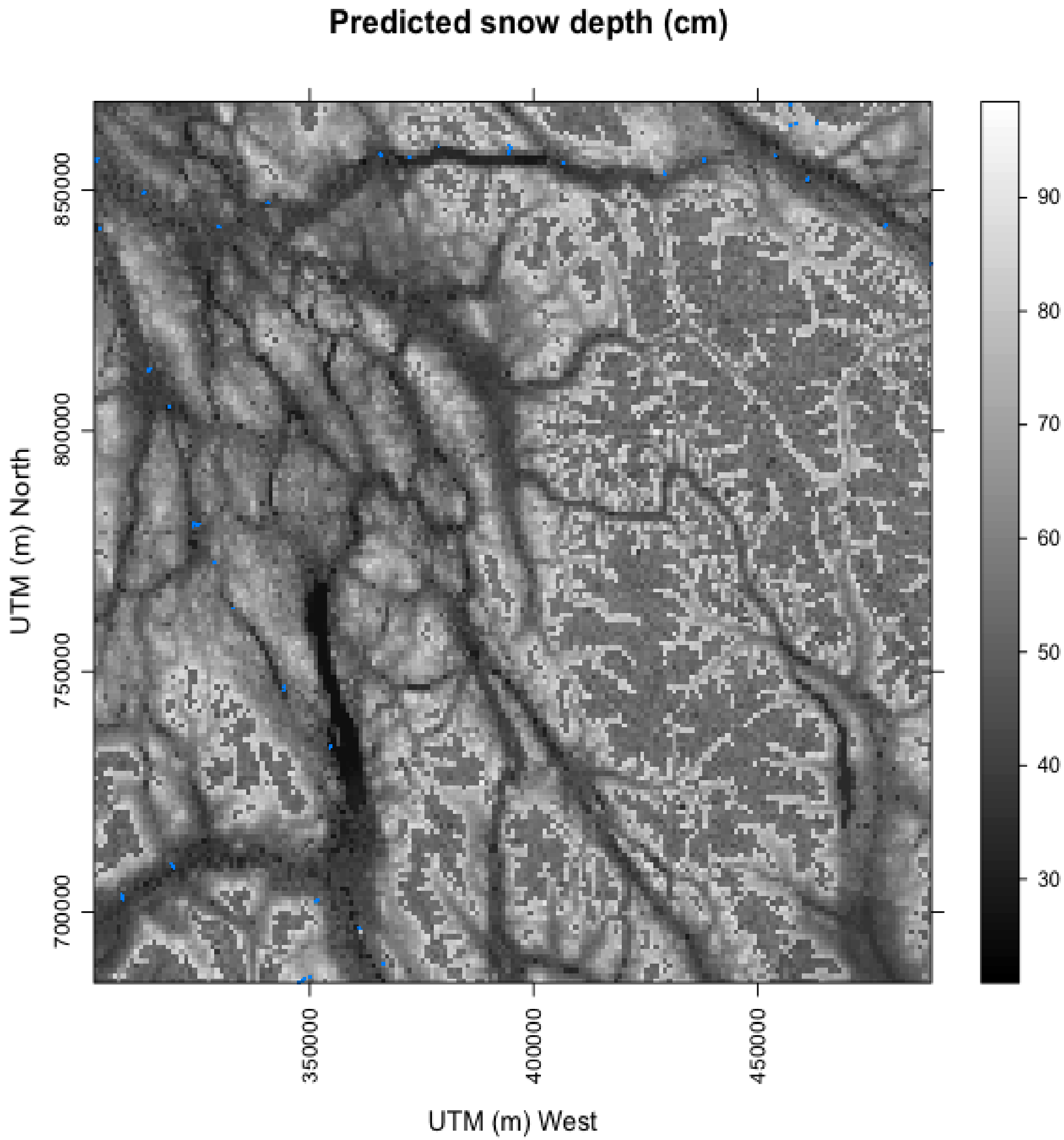

Figure 5.12: Predicted snow depth for central Yukon (2008) in cm. Coordinates are UTM map coordinates in meters. Actual survey sites are shown as blue dots.

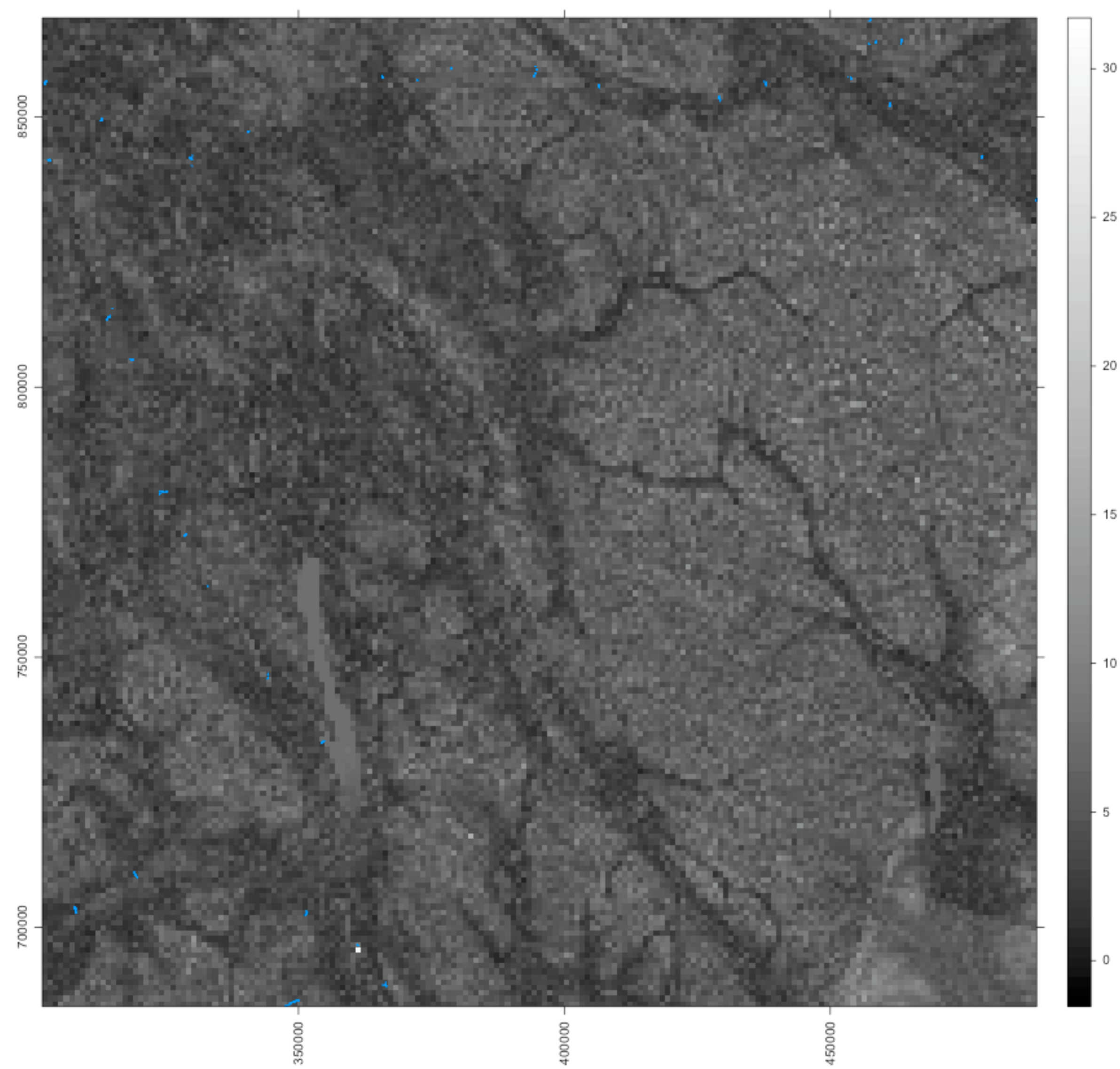

Figure 5.13: A map of confidence in prediction. The numeric value is the sum of the number standard deviations a gridcell's variables exceed the mean of the field data set. The field data set has a range of 0.722,–13.4, with a mean of 4.29

5.8 Map of snow water equivalent

The common approach to modelling SWE when SD is the primary measured variable is to form a linear regression between SD and SWE for each area of the model, such as sub-basins or transects. This was justified as SWE has been found to be much less spatially variable than SD (Elder et al., 1991; Pomeroy & Gray, 1995; Leydecker et al., 2001; Derksen et al., 2005; Erxleben et al., 2002; Winstral et al., 2002; Plattner et al., 2006), particularily after ripening. As the measurements in this study were made at end of season, but before melt, a maximum uniformity from seasonal metamorphism is expected (Pomeroy & Gray, 1995).

In the same manner as for SD, a MER model (Table 5.7) was built for density on the snow pit and density samples. This model was then used to predict density for each SD prediction in the study region, giving a final SWE map (Figure 5.14).

As no regression model for SWE could be derived with the available data set to a sufficient standard of quality, it is recommended that mean density over the whole study area, or mean density by land cover class, be used to convert SD to SWE.

Final SWE model

	term	value
Weighting paramters	power	
Fixed effect coefficents	lc_satConiferous (cm)	
	lc_satDecidious (cm)	
	lc_satWater (cm)	
	lc_satBurn (cm)	
	ts_green_X (DN)	
	hcurv (rad/m)	
	aspect_sin_X (cos(degrees))	
	solrad_X (Wh/m2)	0.000
	elev (m)	
	elev_lctree (m)	-0.000
Random effect coefficents	SDyear (cm)	0.000
	SDtransect (cm)	0.000
	SDsite (cm)	0.027
	SDres (cm)	0.033
Predictive performance	rmse_fit1 (cm)	0.041
	rsq_fit1	0.400
	mbe1	0.002

Table 5.7: Final model for snow water equivalent (mm)

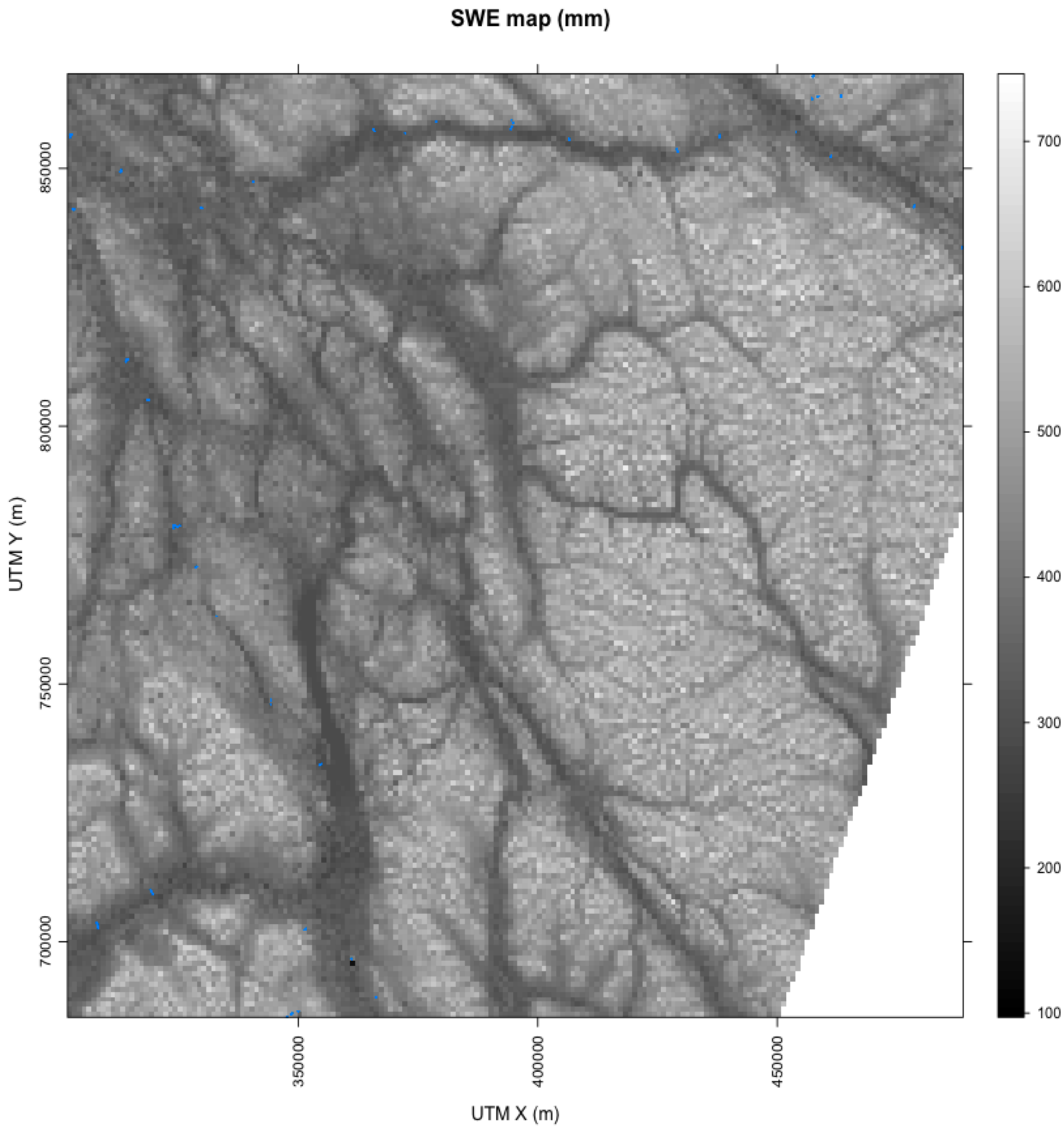

Figure 5.14: Predicted snow water equivalent for central Yukon (2008) in mm. Coordinates are UTM map coordinates in meters. Actual density survey sites are shown as blue dots.

5.9 Summary

The final MER model and its intermediate steps were described, and the assumptions of the MER model were checked. Then the final SD map was produced. The same process was used to create a SWE model on the density and snow pit data, and this model was used to convert the SD map into a SWE map.

Chapter 6

Discussion

6.1 Conclusions

Through mixed effects regression a SD and SWE map for the central Yukon has been produced. In constructing this map, the assumptions required of the mixed effects model have not been violated, and so the final product is statistically robust. The model indicates that SD was primarily predicted by elevation, but that land cover, and shelter contribute.

Previous regressions with sampling less than the range of autocorrelation violate the independence assumptions (Erickson et al., 2005). All previous regressions with sampling with spacing greater than the autocorrelation range miss the small scale variation of SD or SWE, a major contributor of its sampling variation. Mixed effects modelling is a requirement to use regression, as evidenced in the different estimations produced by the GLS model. Some assumptions are still violated, however, although it is considered that the violations are of a non-critical nature and which adds to the error of the estimates, rather than invalidates the findings. $R^2$is a poor measure for goodness of fit of an autocorrelated model as it will be inflated. However, its simplicity has encouraged its use in a wide variety of snow models, and so to allow inter-comparability, it has been included here.

Many studies conclude that SD is related to SWE, and its ease of measurement makes it the preferred observation variable in the field. Measuring SWE directly could increase the accuracy of the model, at a cost of vastly increased time (at least six times longer). SD is strongly related to elevation, as shown in a number of previous studies. This indicates the transferability of this result is high.

6.2 Discussion

6.2.1 SD model interpretation

Examining the SD map, some conclusions about the performance of the model can be drawn. The transition from normal model behaviour in the low-middle elevations is consistent, but the shift into the higher elevations is very abrupt. This is due to the influence of the $isforest$ variable. With enough sampling above the treeline this variable ought to become unnecessary, as the regression fits will adjust to the aspect and wind shelter information to properly strip the mountain tops.

In addition, due to the configuration of the random effects to only influence the intercept, the snow distribution generated is identical for both model years, with only the intercept changing. This adds the assumption that the effect of each parameter is fixed for all years. This requires more data, especially in a low snow year, to properly evaluate.

Terms included in the model are typical of those found in other regression based studies (see chapter 2.4.2). Elevation is the dominant factor, however, it's effects are mitigated at higher elevation, and where there is water. This indicates that the large impact of elevation requires some sort of land cover based shelter. Landcover in this model enters in two ways, through the tassel cap variables brightness (highlighting urban, and bare surfaces), and greenness (vegetation). The second mode of vegetation in the model is through the classified image as a weighting parameter. This weighting indicates a significant difference in the snow distribution under these different land covers. With the variability of snow distribution in coniferous forests set to 1, all other land covers have less variability, with water at 45%. It seems that the coniferous forests have the most variable snow distribution. This is likely due to the presence of tree wells, depressions forming around the base of the trees. The second most variable, burn, also had a very chaotic ground cover. The inclusion of a power term in the weighting chapter indicates that variability increased as SD increased, non-linearly.

6.2.2 Modelling choices

Overall the MER model has performed well. The result is simple, and able to predict the end of season snow accumulation (SD) in the study region. The prediction surface is smooth, unlike one that would be produced by a tree based approach. The spatial autocorrelation structure of SD is accounted for, unlike in a basic regression, and allows for repeat observations on the same site, characterizing both local and regional variability. The distribution of the sampling sites did not unduly impact the results, as location information was not used in the prediction, unlike with a kriging estimator.

The use of the 'reduction in sum of standard errors of predictor variables' as a selection criteria proved relatively inconsequential, as selection using the BIC produced the same subset. However, due to the potential problems with the BIC and the MER model, the chosen criteria is still preferred.

The existence of a strong relationship between elevation and SD would allow the development of a co-kriging model, however this was beyond the purpose of this study. Likewise, the existence of non-linear relationships in the SD model would justify the use of a GAM, particularly the shape of the scatterplot for elevation, however the complexity of simultaneously fitting a GAM and MER (a GA Mixed Model (GAMM)) was beyond the scope of this study. In addition, the random effects are not as easily interpreted (R help files, mgcv package, v1.5-5).

The added difficulty in building a MER model compared to any other of the described approaches is not large, with the exception of a simple linear regression. The added benefits in study design and in meeting the methodological assumptions are too great not to undertake.

Table 6.1 summarizes the accuracy of a number of similar studies, predicting SD and SWE. It can be seen that this study falls into the general range of accuracy, however the area covered by the study is larger than all but Lopez-Moreno & Nogues-Bravo (2006).

Accuracies of similar studies

Study	Location	Mean SD (cm)	RMSE of SD prediction
This study	Central Yukon	0.39	0.5
Erxleben et al. (2002)	St. Louis creek	58	10.4
Erxleben et al. (2002)	Fool creek	109	17.5
Erxleben et al. (2002)	Walton creek	177	31.3
Jost et al. (2007)	Cotton Creek	10.75–28.93	8.77–10.45
Molotch et al. (2005)	Tokopah Basin	255	77.64
Lopez-Moreno & Nogues-Bravo (2006)	Spanish Pyrenees	approx. 90	27.5
Winstral et al. (2002)	Green Lake 4	227	approx 40

Table 6.1: Accuracies of similar regression based studies.

6.2.3 Applications

The final product of this study, a SD map for the central Yukon can provide other researchers with a significantly more detailed product for their work. As a validation dataset for passive microwave algorithms, the map will be partially successful. The lack of high-altitude predictions will have a strong impact, as passive microwave observations are large in footprint, and will likely contain an amount of this unknown area. As proposed below in the further work, it may be possible to extend this model into these areas.

6.3 Limitations

6.3.1 Sources of Error

There are several potential sources of error for this model. The most probable are an error in the model function, as insufficient data points were acquired to test higher order interaction terms or polynomial transformations. Thus, theoretically, an ideal model with perfectly parameterized terms could not have been tested. The 8-10 year gap between image acquisition and field use may have led to some sites being classified under different conditions than they were sampled. One Landsat scene (lower left, WRS2 coordinates 61-17) was hazy which produced different DNs for the transformations and classification.

A major probable mis-specification in the model was the lack of a wind term. While the effects of wind on snow are mitigated by sheltering terrain (included via elevation range, horizontal and profile curvature, elevation standard deviation), and vegetation (both classification and transformation express increasing capture capability), the directional effects were not explored. For example, relying on confounders can only increase the complexity of the model.

Inter-variable correlation is problematic in this data set. Vegetation is elevation dependant, with conifers in the valleys, deciduous on the slopes, and no trees on the peaks. Interception in the conifers might negatively influence snowpack accumulation, also enhancing the positive trend with elevation.

The effects of shrinkage, the over-fitting of regression coefficients, were not examined directly. Examining the cross-validation estimates for the coefficients, the degree of variance indicates that over-fitting was present, but the small RMSE indicates that it is not large. Royston et al. (2008) summarize a number of studies on the topic of sample size. A sample of 10 events per variable is concluded as the minimum to avoid having significant shrinkage, however, multi-level studies were not discussed. Pinheiro & Bates (2000) state that the pooling effect of MER should add robustness against shrinkage. This study includes 14 variables, along with a transformation for 11 of them, so should have a minimum of 140-260 observations. If taken at the site level, there are 214 observations, which unlikely to be sufficient, however, approximately 20 measurements make up each observation. Due to this a selection bias might be expected, causing weakly correlated predictors to not be selected, and shrinkage, the mis-estimation of the model parameters to be present, although these effects are likely to be minimal. These effects will be concentrated on variables that contribute least to the model (Royston et al., 2008).

6.4 Recommendations

Further work to improve the estimates of this model should include sampling SWE (density) more intensively, and locating the samples at the corners of the study site triangles rather than only at the center, so as to improve the within-site scale variance estimate; effectively only the 1 m and 100 m variance were measured, not the 30 m (see Watson et al. (2006)).

Furthermore, the model should include a measure of wind directly which has been used frequently in regression models by other authors. Its inclusion makes increasing physical sense at higher altitudes where wind scouring and drifting play an important role (Elder et al., 1991).

Finally, additional surveying of SD and density to increase the sample size. This would allow us to increase the number of possible regressors or interactions considered, and increase the accuracy of the prediction. Doing so will vastly improve the usefulness of these results to other researchers.

References

Anderton, S., White, S., & Alvera, B. (2004). Evaluation of spatial variability in snow water equivalent for a high mountain catchment. *Hydrological Processes*, *18*(3), 435–453.

Blöschl, G. (1999). Scaling issues in snow hydrology. *Hydrological Processes*, *13*, 2149–2175.

Brabets, T., Wang, B., Meade, R., & Geological Survey, A. W. R. D. D. . ., Anchorage (2000). Environmental and hydrologic overview of the Yukon River Basin, Alaska and Canada. Tech. Rep. 99–4204, United States Geological Survey.

Breiman, L., Friedman, J. H., Olshen, R. A., & Stone, C. J. (1984). *Classification and regression trees*. Chapman & Hall/CRC.

Brenning, A., Kaden, K., & Itzerott, S. (2006). Comparing classifiers for crop identification based on multitemporal Landsat TM/ETM data. In *2nd Workshop of the EARSeL Special Interest Group on Land Use & Land Cover, CD-ROM*.

Brenning, A., Piotraschke, H., & Leithold, P. (2008). Geostatistical analysis of on-farm trials in Precision Agriculture. *Proceedings, GEOSTATS*, (pp. 1–5).

Carroll, S., & Cressie, N. (1997). Spatial modeling of snow water equivalent using covariances estimated from spatial and geomorphic attributes. *Journal of Hydrology*, *190*(1-2), 42–59.

Cline, D., Armstrong, R., Davis, R., Elder, K., & Liston, G. (2001). NASA Cold Land Processes Field Experiment Plan 2002-2004. *Cold Land Processes Working Group, NASA Earth Science Enterprise. Land Surface Hydrology Program*, (p. 202).

Corripio, J., & Purves, R. (2005). Surface energy balance of high altitude glaciers in the Central Andes: the effect of snow penitentes. *Climate and hydrology in mountain areas*, (pp. 15–27).

Cressie, N. (1991). *Statistics for spatial data*. John Wiley & Sons, New York.

Demidenko, E. (2005). *Mixed models: theory and applications*. Wiley-Interscience.

Derksen, C., Walker, A., Goodison, B., & Strapp, J. (2005). Integrating in situ and multiscale passive microwave data for estimation of subgrid scale snow water equivalent distribution and variability. *IEEE Transactions on Geoscience and Remote Sensing*, *43*(5), 960–972.

Derksen, C., Walker, A., & Toose, P. (2007). *Estimating snow water equivalent in northern regions from satellite passive microwave data*. Springer.

Elder, K., Cline, D., Liston, G. E., & Armstrong, R. (2009). NASA Cold Land Processes Experiment (CLPX 2002/03): Field Measurements of Snowpack Properties and Soil Moisture. *Journal of Hydrometeorology*, *10*(1), 320–329.

Elder, K., Dozier, J., & Michaelsen, J. (1991). Snow accumulation and distribution in an alpine watershed. *Water Resourources Research*, *27*(7), 1541–1552.

Elder, K., Rosenthal, W., & Davis, R. E. (1998). Estimating the spatial distribution of snow water equivalence in a montane watershed. *Hydrological Processes*, *12*(10-11), 1793–1808.

Erickson, T., Williams, M., & Winstral, A. (2005). Persistence of topographic controls on the spatial distribution of snow in rugged mountain terrain, Colorado, United States. *Water Resources Research*, *41*(4), W04014.

Erxleben, J., Elder, K., & Davis, R. (2002). Comparison of spatial interpolation methods for estimating snow distribution in the Colorado Rocky Mountains. *Hydrological Processes*, *16*(18), 3627—3649.

Essery, R., Li, L., & Pomeroy, J. (1999). A distributed model of blowing snow over complex terrain. *Hydrological processes*, *13*, 2423–2438.

Faraway, J. (2006). *Extending the linear model with R: generalized linear, mixed effects and nonparametric regression models*. Chapman & Hall/CRC.

Fassnacht, S., & Deems, J. (2006). Measurement sampling and scaling for deep montane snow depth data. *Hydrological Processes*, *20*(4), 829—838.

Harrell Jr., F., Lee, K., Califf, R., Pryor, D., & Rosati, R. (1984). Regression modelling strategies for improved prognostic prediction. *Statistics in Medicine*, *3*(2), 143 –152.

Hedstrom, N., & Pomeroy, J. (1998). Measurements and modelling of snow interception in the boreal forest. *Hydrological Processes*, *12*, 1611–1625.

Herzfeld, U., Mayer, H., Caine, N., Losleben, M., & Erbrecht, T. (2003). Morphogenesis of typical winter and summer snow surface patterns in a continental alpine environment. *Hydrological Processes*, *17*(3), 619—649.

Janowicz, J., Richard; Joe-Strack (2008). Yukon snow survey bulletin and water supply forecast. Tech. rep., Environment Yukon - Water Resources Branch.

Jensen, J. R. (2007). *Remote sensing of the environment: an earth resource perspective*. Prentice Hall, 2 ed.

Jost, G., Weiler, M., Gluns, D. R., & Alila, Y. (2007). The influence of forest and topography on snow accumulation and melt at the watershed-scale. *Journal of Hydrology*, *347*(1-2), 101 – 115.

Lapena, D. R., & Martz, L. W. (1996). An investigation of the spatial association between snow depth and topography in a prairie agricultural landscape using digital terrain analysis. *Journal of Hydrology*, *184*(3-4), 277 – 298.

Leydecker, A., Sickman, J. O., & Melack, J. M. (2001). Spatial scaling of hydrological and biogeochemical aspects of high-altitude catchments in the sierra nevada, california, u.s.a. *Arctic, Antarctic, and Alpine Research*, *33*(4), 391–396.

Li, L., & Pomeroy, J. (1997). Probability of occurrence of blowing snow. *Journal of Geophysical Research-Atmospheres*, *102*(D18), 21955–21964.

Liston, G., & Elder, K. (2006). A distributed snow-evolution modeling system (SnowModel). *Journal of Hydrometeorology*, *7*(6), 1259–1276.

Liston, G., Haehnel, R., Sturm, M., Hiemstra, C., Berezovskaya, S., & Tabler, R. (2007). Instruments and Methods: Simulating complex snow distributions in windy environments using SnowTran-3 D. *Journal of Glaciology*, *53*(181), 241–256.

Liston, G., & Sturm, M. (1998). A snow-transport model for complex terrain. *Journal of Glaciology*, *44*(148), 498–516.

Liston, G., & Sturm, M. (2002). Winter precipitation patterns in arctic Alaska determined from a blowing-snow model and snow-depth observations. *Journal of hydrometeorology*, *3*(6), 646–659.

Lopez-Moreno, J., & Nogues-Bravo, D. (2006). Interpolating local snow depth data: an evaluation of methods. *Hydrological Processes*, *20*(10), 2217–2232.

López-Moreno, J., & Stähli, M. (2008). Statistical analysis of the snow cover variability in a subalpine watershed: Assessing the role of topography and forest interactions. *Journal of Hydrology*, *348*(3-4), 379–394.

López-Moreno, J., Vicente-Serrano, S., & Lanjeri, S. (2007). Mapping snowpack distribution over large areas using GIS and interpolation techniques. *Climate Research*, *33*(3), 257.

Luce, C., Tarboton, D., & Cooley, K. (1998). The influence of the spatial distribution of snow on basin-averaged snowmelt. *Hydrological Processes*, *12*(10), 1671–1683.

Luce, C., Tarboton, D., & Cooley, K. (1999). Sub-grid parameterization of snow distribution for an energy and mass balance snow cover model. *Hydrological Processes*, *13*(12), 1921–1933.

Lyles, L., & Allison, B. (1976). Wind erosion: the protective role of simulated standing stubble. *Transactions ASAE*, *19*(1), 61–64.

Marshall, H., Koh, G., Sturm, M., Johnson, J., Demuth, M., Landry, C., Deems, J., & Gleason, J. (2006). Spatial variability of the snowpack: Experiences with measurements at a wide range of length scales with several different high precision instruments. In *Proceedings ISSW*, (pp. 1–6).

Molotch, N., Colee, M., Bales, R., & Dozier, J. (2005). Estimating the spatial distribution of snow water equivalent in an alpine basin using binary regression tree models: the impact of digital elevation data and independent variable selection. *Hydrological Processes*, *19*(7), 1459–1479.

Montesi, J., Elder, K., Schmidt, R., & Davis, R. (2004). Sublimation of intercepted snow within a subalpine forest canopy at two elevations. *Journal of Hydrometeorology*, *5*(5), 763–773.

Pinard, J., Benoit, R., & Yu, W. (2005). A WEST wind climate simulation of the mountainous Yukon. *Atmosphere-Ocean*, *43*(3), 259–282.

Pinheiro, J. C., & Bates, D. M. (2000). *Mixed-effects models in S and S-PLUS*. Springer-Verlag.

Plattner, C., Braun, L. N., & Brenning, A. (2006). The spatial variability of snow accumulation on Vernagtferner, Austrian Alps, in winter 2003/2004. *Zeitschrift für Gletscherkunde und Glazialgeologie*, *39*, 43–57.

Pomeroy, J. (1989). A process-based model of snow drifting. *Annals of Glaciology*, *13*, 237–240.

Pomeroy, J., & Li, L. (2000). Prairie and Arctic areal snow cover mass balance using a blowing snow model. *Journal of Geophysical Research-Atmospheres*, *105*(D21), 26619–26634.

Pomeroy, J. W., Gray, D. M., & Landine, P. G. (1993). The prairie blowing snow model: Characteristics, validation, operation. *Journal of Hydrology*, *144*(1-4), 165–192.

Pomeroy, W., J, & Gray, M., D (1995). *Snowcover: Accumulation, Relocation and Management.*, vol. 88. Supply and Services Canada, Saskatoon.

Royston, P., Sauerbrei, W., & InterScience, W. (2008). *Multivariable model-building: A pragmatic approach to regression analysis based on fractional polynomials for modelling continuous variables*. John Wiley.

Stahli, M., Schaper, J., & Papritz, A. (2002). Towards a snow-depth distribution model in a heterogeneous subalpine forest using a Landsat TM image and an aerial photograph. *Annals of Glaciology*, *34*, 65–70.

Trujillo, E., Ramirez, J. A., & Elder, K. J. (2009). Scaling properties and spatial organization of snow depth fields in sub-alpine forest and alpine tundra. *Hydrological Processes*, *23*(11), 1575–1590.

Watson, F., Newman, W., Coughlan, J., & Garrott, R. (2006). Testing a distributed snowpack simulation model against spatial observations. *Journal of Hydrology*, *328*(3-4), 453–466.

Watson, F. G. R., Anderson, T. N., Newman, W. B., Alexander, S. E., & Garrott, R. A. (2006). Optimal sampling schemes for estimating mean snow water equivalents in stratified heterogeneous landscapes. *Journal of Hydrology*, *328*(3-4, Sp. Iss. SI), 432–452.

Wilson, J., & Gallant, J. (2000). *Terrain analysis: principles and applications*. Wiley.

Winkler, R., Spittlehouse, D., & Golding, D. (2005). Measured differences in snow accumulation and melt among clearcut, juvenile, and mature forests in southern British Columbia. *Hydrological processes*, *19*(1), 51–62.

Winstral, A., Elder, K., & Davis, R. (2002). Spatial snow modeling of wind-redistributed snow using terrain-based parameters. *Journal of Hydrometeorology*, *3*(5), 524–538.

Appendix A

Methods

A.1 Stepwise LME fitting function

```
function (model, data, scope, start = NA, direction = "forward",
    steps = 1000, verbose = T, makeVars = F)
{
    failfm = list(0)
    testedfm = list(0)
    tests = 0
    pred = as.character(scope[2])
    terms = paste("+", gsub(" ", "", strsplit(as.character(scope[3]),
        "+", fixed = T)[[1]]))
    bestmodel = model
    bestmodelF = 0
    stillsearching = T
    stoppingP = 0.05
    stoppingP = 1 - (1 - stoppingP)^(1/sum(seq(length(terms),
        1)))
    vc = VarCorr(bestmodel)
    intercepts = which(rownames(vc) == "(Intercept)")
    resids = which(rownames(vc) == "Residual")
    SDI = sqrt(sum(as.numeric(vc[c(intercepts), 1])))
    SDR = sqrt(sum(as.numeric(vc[c(resids), 1])))
    SDtot = sqrt(sum(SDI^2, SDR^2))
    bestSD = SDtot
    gainSD = 0
    haschanged = F
    if (!is.na(start)) {
```

```
    if (verbose)
        print("Starting formula provided, fitting and continuing.")
    tryCatch({
        bestmodel <- update(model, fixed = start)
    }, error = function(e) {
        if (verbose)
            print("         Caught an error")
        print(e)
        failfm <- append(failfm, RHS)
        error <- T
    })
    if (direction == "both") {
        termsbest = strsplit(as.character(formula(bestmodel)[3]),
            "+", fixed = T)[[1]]
        termsbest = strsplit(termsbest, "-", fixed = T)
        termsbest = unlist(termsbest)
        termsbest = gsub(" ", "", termsbest)
        if (length(grep("1", termsbest)) == 0)
            termsbest = append(termsbest, "intercept")
        terms = append(paste("+", gsub(" ", "", strsplit(as.character(scope[3]),
            "+", fixed = T)[[1]])), "+ 1")
        for (k in termsbest) {
            k = paste("+", k)
            if (k == "+ 1") {
              if (verbose)
                print("Re-adding intercept")
              next
            }
            if (k == "+ intercept") {
              k = "+ 1"
              if (verbose)
                print("Dropping intercept")
            }
            terms[terms == k] = gsub("+", "-", terms[terms ==
              k], fixed = T)
        }
    }
}
for (j in 1:min(length(terms), steps)) {
    if (verbose)
```

```
    print(paste(j, "==================================================
curmodel = bestmodel
curfm = formula(curmodel)
curR = data.frame(term = terms, F = 0, SDI = 10000, SDR = 10000,
    SDt = 10000)
tempbestmodel = bestmodel
tempbestmodelF = 0
tempbestmodelP = 1
tempbestmodelSDt = 100000
lastTermAdded = NA
haschanged = F
for (i in terms) {
    curfm = formula(curmodel)
    term = gsub("+ ", "", i, fixed = T)
    term = gsub("- ", "", term, fixed = T)
    testfm = as.character(curfm)[3]
    temp = paste(as.character(curfm)[c(2, 1)], collapse = "")
    testfm = paste(temp, testfm)
    testfm = formula(paste(testfm, i))
    temp = as.character(testfm)[3]
    if (length(grep("- 1", temp, fixed = T)) == 1 & length(grep("+ 1",
        temp, fixed = T)) == 1) {
        if (verbose)
          print("     adjusting FM.")
        temp = gsub(" + 1", "", temp, fixed = T)
        temp = gsub(" - 1", "", temp, fixed = T)
        testfm = paste(testfm[c(2, 1)], collapse = "")
        testfm = gsub("`", "", testfm)
        testfm = formula(paste(testfm, temp, collapse = ""))
    }
    if (verbose)
        print(paste("Testing:", paste(testfm[c(2, 1,
          3)], collapse = "")))
    RHS = paste(sort(gsub(" ", "", strsplit(as.character(testfm[3]),
        "+", fixed = T)[[1]])), collapse = "+")
    if (!is.na(match(RHS, testedfm))) {
        if (verbose)
          print(paste("          AlreadyTested:", RHS))
        next
    }
```

```
testedfm <- append(testedfm, RHS)
if (!is.na(match(RHS, failfm))) {
    if (verbose)
      print(paste("         Skipping-failedprev:",
        RHS))
    next
}
tests = tests + 1
error = F
tryCatch({
    curmodel <- update(bestmodel, fixed = testfm)
}, error = function(e) {
    if (verbose)
      print("         Caught an error")
    print(e)
    failfm = append(failfm, RHS)
    error = T
})
if (error)
    next
haschanged = T
a = anova(curmodel)
termrange = 1
if (nrow(a) > 1)
    termrange = 2:nrow(anova(curmodel))
tryCatch({
    a_all = anova(curmodel, Terms = termrange)
    thisallF = a_all[, 3]
}, error = function(e) {
    if (verbose)
      print("         Caught an error")
    print(e)
    a_all = NA
    thisallF = NA
    error = T
})
thisF = a[match(term, rownames(a)), 3]
thisP = a[match(term, rownames(a)), 4]
vc = VarCorr(curmodel)
intercepts = which(rownames(vc) == "(Intercept)")
```

```
    resids = which(rownames(vc) == "Residual")
    SDI = sqrt(sum(as.numeric(vc[c(intercepts), 1])))
    SDR = sqrt(sum(as.numeric(vc[c(resids), 1])))
    SDtot = sqrt(sum(SDI^2, SDR^2))
    if (SDtot < min(curR$SDt)) {
        if (verbose)
          print("         temp_best")
        tempbestmodel = curmodel
        tempbestmodelF = thisallF
        tempbestmodelP = thisP
        tempbestmodelSDt = SDtot
    }
    curR[match(i, terms), ] = data.frame(term = i, F = thisallF,
        SDI, SDR, SDt = SDtot)
    curmodel = bestmodel
    if (verbose)
        print(paste("         F:", thisallF, "-:", thisP,
          "SDI:", SDI, "SDR:", SDR, "SDtot:", SDtot))
}
termAdded = paste(curR[which.min(curR$SDt), "term"])
if (verbose)
    print("~~~~~~~~~")
if (verbose)
    print(paste("Best term: ", termAdded))
if (verbose)
    print(paste("Total model SDt:", tempbestmodelSDt))
if (verbose)
    print(paste("Best model SDt:", bestSD))
gainSD = bestSD - tempbestmodelSDt
if (T | gainSD > 0.1) {
    bestSD = tempbestmodelSDt
    bestmodel = tempbestmodel
    bestmodelF = tempbestmodelF
    bestmodelSDt = tempbestmodelSDt
    if (verbose)
        print(paste("New best model, bestSD", bestSD,
          "gain:", gainSD))
}
else {
    if (verbose)
```

```
        print("stopping")
    stillsearching = F
}
a = anova(bestmodel)
if (!is.na(lastTermAdded)) {
    if (a[match(lastTermAdded, rownames(a)), 4] > stoppingP) {
        if (verbose)
          print(paste("We should drop the previous added term. (but we wont)",
            lastTermAdded))
    }
}
print(a)
if (direction == "both") {
    termsbest = strsplit(as.character(formula(bestmodel)[3]),
        "+", fixed = T)[[1]]
    termsbest = strsplit(termsbest, "-", fixed = T)
    termsbest = unlist(termsbest)
    termsbest = gsub(" ", "", termsbest)
    if (length(grep("1", termsbest)) == 0)
        termsbest = append(termsbest, "intercept")
    terms = append(paste("+", gsub(" ", "", strsplit(as.character(scope[3]),
        "+", fixed = T)[[1]])), "+ 1")
    for (k in termsbest) {
        k = paste("+", k)
        if (k == "+ 1") {
          if (verbose)
            print("Re-adding intercept")
          next
        }
        if (k == "+ intercept") {
          k = "+ 1"
          if (verbose)
            print("Dropping intercept")
        }
        terms[terms == k] = gsub("+", "-", terms[terms ==
          k], fixed = T)
    }
}
else terms = terms[-term]
thisF = thisP = thisallF = 0
```

```
        lastTermAdded = termAdded
        if (!stillsearching)
            break
        if (!haschanged)
            break
    }
    if (makeVars)
        stepwiseLME.failfm <<- failfm
    if (makeVars)
        stepwiseLME.tests <<- tests
    return(bestmodel)
}
```

Appendix B

Software and data

B.1 Software

GIS: ArcGIS v9.2 SAGA GIS v2.0.3
Statistics: R v2.9.0 RSAGA v0.9-5 nlme v 3.1-92

B.2 Data

Geomatics Yukon, Information & Communication Technologies Division Department of Highways and Public Works; http://www.geomaticsyukon.ca/index.html

1. Digital elevation model: 90 m resolution, whole Yukon coverage. GeoTiff format. http://www.geomaticsyukon.ca/data_download.html#elevation

2. Landsat imagery: 30m resolution, 7 bands. ftp://ftp.geomaticsyukon.ca/Imagery/Landsat7/Scenes/

Appendix C

Results

C.1 Final Model: SD

```
Linear mixed-effects model fit by REML
 Data: data[data$pred, ]
    AIC   BIC logLik
  27060 27173 -13512

Random effects:
 Formula: ~1 | year
        (Intercept)
StdDev:         8.7

 Formula: ~1 | mergetrans \%in\% year
        (Intercept)
StdDev:         6.6

 Formula: ~1 | site \%in\% mergetrans \%in\% year
        (Intercept) Residual
StdDev:      0.0082      1.1

Correlation Structure: Spherical spatial correlation
 Formula: ~x + y | year/mergetrans/site
 Parameter estimate(s):
 range nugget
 69.71   0.21
Combination of variance functions:
 Structure: Different standard deviations per stratum
```

```
 Formula: ~1 | lc_sat
 Parameter estimates:
conif  burn water decid
 1.00  0.81  0.45  0.83
 Structure: Power of variance covariate
 Formula: ~fitted(., level = 1)
 Parameter estimates:
power
 0.66
Fixed effects: chooseCVfm(fit.step.cvrefit.summaries)
                     Value Std.Error   DF t-value p-value
(Intercept)             40         7 3733     5.9  0.0000
hcurv                 1292       321 3733     4.0  0.0001
aspect_sin_X            -1         1 3733    -0.9  0.3913
elev_rng_log             1         1 3733     1.9  0.0608
ts_bright_X              0         0 3733    -5.6  0.0000
ts_green_X               0         0 3733     3.7  0.0003
elev_X:isforestFALSE     0         0 3733     2.2  0.0314
elev_X:isforestTRUE      0         0 3733     7.8  0.0000
 Correlation:
                     (Intr) hcurv  asp__X elv_r_ ts_b_X ts_g_X e_X:FA
hcurv                 0.019
aspect_sin_X         -0.145 -0.064
elev_rng_log         -0.265 -0.001  0.110
ts_bright_X          -0.225 -0.016 -0.070  0.049
ts_green_X           -0.170 -0.020  0.027 -0.060  0.439
elev_X:isforestFALSE -0.026 -0.086 -0.069 -0.156 -0.154 -0.071
elev_X:isforestTRUE  -0.053  0.023 -0.048 -0.314  0.182 -0.103  0.548

Standardized Within-Group Residuals:
   Min     Q1    Med     Q3    Max
-4.379 -0.370  0.072  0.488  6.808

Number of Observations: 3924
Number of Groups:
                          year           mergetrans \%in\% year
                             2                               50
site \%in\% mergetrans \%in\% year: 184
```

C.2 Final Model: SWE

```
Linear mixed-effects model fit by REML
 Data: pit
    AIC   BIC logLik
  -1174 -1131    598

Random effects:
 Formula: ~1 | year
        (Intercept)
StdDev:  0.00000093

 Formula: ~1 | mergetrans \%in\% year
        (Intercept)
StdDev:       2e-11

 Formula: ~1 | site \%in\% mergetrans \%in\% year
        (Intercept) Residual
StdDev:       0.027    0.033

Fixed effects: chooseCVfm(fit.step.swe.cvrefit.summaries, predvar = "density")
                   Value Std.Error  DF t-value p-value
(Intercept)          0.1       0.0 227     3.9  0.0001
vcurv                9.9       4.4  78     2.3  0.0265
solrad               0.0       0.0  78     1.1  0.2690
solrad_X             0.0       0.0  78     3.1  0.0024
ts_bright_X          0.0       0.0  78     0.2  0.8178
elev:isforestFALSE   0.0       0.0  78     1.5  0.1275
elev:isforestTRUE    0.0       0.0  78    -1.2  0.2203
 Correlation:
                   (Intr) vcurv  solrad slrd_X ts_b_X e:FALS
vcurv               0.577
solrad             -0.934 -0.553
solrad_X            0.344  0.689 -0.272
ts_bright_X        -0.125  0.149 -0.061  0.098
elev:isforestFALSE  0.045 -0.169 -0.231 -0.359 -0.321
elev:isforestTRUE  -0.063 -0.126 -0.268 -0.394  0.268  0.670

Standardized Within-Group Residuals:
  Min    Q1   Med    Q3   Max
```

```
-1.82 -0.56 -0.17  0.41  3.62

Number of Observations: 361
Number of Groups:
                          year           mergetrans \%in\% year
                             2                               50
site \%in\% mergetrans \%in\% year
                           134
```

Appendix D

Data summary

	record	counter	year	mergetrans	site	numsats	altde	depthvolts	lat	lon
2008/T12	7593.70	120069.70	2008	T12	002	8.81	875.45	2.90	60.68	-134.95
2008/T45	7779.17	450101.17	2008	T45	10006	10.97	1179.85	2.88	60.64	-135.26
2008/T46	8088.59	460175.59	2008	T46	013	10.49	690.88	1.97	60.78	-136.02
2008/T47	8487.13	470097.13	2008	T47	019	10.92	678.65	1.67	60.84	-135.82
2008/T05	8711.41	50058.41	2008	T05	028	11.00	629.24	1.13	61.08	-135.19
2008/T48	8954.34	480096.34	2008	T48	038	10.37	706.18	2.72	61.48	-135.79
2008/T49	9105.21	490053.21	2008	T49	040	10.81	907.92	2.91	61.41	-135.71
2008/T03	9242.00	30013.00	2008	T03	042	10.90	622.36	2.44	61.70	-135.93
2008/T02	9354.61	24511.92	2008	T02	048	9.34	603.23	3.11	61.76	-136.02
2008/T50	9536.49	500059.49	2008	T50	051	10.77	1319.60	6.47	62.27	-133.21
2008/T31	9769.40	310086.40	2008	T31	053	9.38	772.81	3.08	62.20	-133.69
2008/T33	10000.27	330047.27	2008	T33	058	9.20	640.46	3.12	62.18	-134.30
2008/T51	10222.65	510054.65	2008	T51	061	8.91	786.19	3.63	62.17	-133.86
2008/T52	10313.34	520036.34	2008	T52	068	10.16	1182.36	5.48	62.30	-133.32
2008/T53	10499.27	530069.27	2008	T53	069	10.07	1058.24	5.07	62.27	-133.31
2008/T54	10649.40	540047.40	2008	T54	073	10.55	803.74	3.13	62.01	-132.71
2008/T15	10782.05	150043.05	2008	T15	077	10.12	780.33	3.21	62.08	-132.91
2008/T25	10945.97	250041.97	2008	T25	081	9.16	748.74	3.09	62.16	-133.24
2008/T55	11065.00	550014.00	2008	T55	085	11.00	685.70	1.69	62.21	-133.39
2008/T34	11136.00	340041.00	2008	T34	088	9.95	641.18	3.25	62.19	-135.08
2008/T56	11288.57	560045.57	2008	T56	090	9.95	639.45	1.93	62.09	-135.55
2008/T38	11424.21	380044.21	2008	T38	095	8.67	568.10	2.75	62.04	-135.76
2008/T40	11564.00	400044.00	2008	T40	096	10.60	544.90	2.93	62.09	-136.08
2008/T41	11715.00	410041.00	2008	T41	100	10.13	658.47	2.79	62.15	-136.29
2008/T59	11906.06	590047.06	2008	T59	105	8.15	542.29	2.84	62.02	-136.26
2008/T57	12128.45	570040.45	2008	T57	108	9.79	838.60	3.25	60.79	-135.23
2008/T58	12282.00	580058.00	2008	T58	114	9.71	649.29	2.75	60.74	-135.04

Table D.1: Summarized field data, part 1a

	record	counter	year	mergetrans	site	numsats	altde	depthvolts	lat	lon
2009/T45	15688.91	1131.22	2009	T45	159	9.58	1302.23	4.38	60.64	-97.36
2009/T46	15520.67	3040.67	2009	T46	164	10.96	699.23	4.07	60.78	-136.02
2009/T47	15641.77	4038.77	2009	T47	168	10.93	679.92	3.36	60.85	-135.82
2009/T12	15746.53	5026.53	2009	T12	171	9.07	871.61	4.33	60.68	-134.95
2009/T05	15796.50	10026.50	2009	T05	172	11.00	628.50	1.44	61.08	-135.19
2009/T1013	15900.19	13028.19	2009	T1013	174	8.21	750.81	2.91	61.18	-135.39
2009/T1015	15986.50	15016.50	2009	T1015	176	11.00	830.42	4.32	61.33	-135.62
2009/T1016	16061.90	16059.90	2009	T1016	177	10.15	562.99	3.34	62.11	-136.32
2009/T49	16148.00	11027.00	2009	T49	179	10.85	911.18	4.62	61.41	-135.71
2009/T48	16315.66	12071.66	2009	T48	182	10.23	707.02	3.59	61.48	-135.80
2009/T03	16424.33	18054.33	2009	T03	185	10.39	621.86	2.02	61.70	-135.93
2009/T59	16533.00	19029.00	2009	T59	189	10.24	564.51	4.13	62.02	-136.26
2009/T1020	16641.80	20028.80	2009	T1020	190	10.07	509.24	3.67	62.82	-136.54
2009/T1021	16694.00	21025.00	2009	T1021	192	11.00	566.21	3.02	62.77	-136.62
2009/T1022	16770.50	22024.50	2009	T1022	194	10.30	539.88	4.17	62.61	-136.85
2009/T41	16822.50	23026.50	2009	T41	197	8.91	641.51	3.25	62.15	-136.29
2009/T40	16875.00	24026.00	2009	T40	198	10.20	545.51	3.28	62.09	-136.08
2009/T56	16923.00	28023.00	2009	T56	200	9.28	638.60	3.63	62.09	-135.55
2009/T50	16990.83	29048.83	2009	T50	203	10.06	1339.73	6.22	62.27	-133.21
2009/T52	17185.63	30065.63	2009	T52	206	10.15	1098.30	5.12	62.30	-133.33
2009/T1031	17292.94	31037.94	2009	T1031	211	10.32	788.00	2.66	61.97	-132.49
2009/T1032	17461.10	32093.10	2009	T1032	214	9.15	769.49	3.84	62.05	-132.84
2009/T1033	17663.74	33079.74	2009	T1033	220	8.47	769.72	4.48	62.20	-134.66

Table D.2: Summarized field data, part 1b

	year	mergetrans	x	y	sd	density.pred	lc_field	lc_sat	elev
2008/T12	2008	T12	366278.31	689278.44	45.22	0.17	forest	conif	883.00
2008/T45	2008	T45	348874.57	686114.48	44.95	0.17	forest	conif	1183.01
2008/T46	2008	T46	308072.95	703183.62	31.04	0.17	burn	decid	686.38
2008/T47	2008	T47	319388.74	709680.36	26.41	0.18	grass	burn	674.95
2008/T05	2008	T05	354648.42	734374.94	18.09	0.21	lake	water	627.00
2008/T48	2008	T48	324768.09	780613.11	42.60	0.17	forest	conif	702.14
2008/T49	2008	T49	328743.47	772686.38	45.50	0.19	burn	burn	907.29
2008/T03	2008	T03	318538.29	805086.73	38.29	0.21	lake	water	627.00
2008/T02	2008	T02	314144.11	812774.37	48.53	0.18	forest	conif	583.05
2008/T50	2008	T50	463336.38	863983.98	100.08	0.20	forest	conif	1317.38
2008/T31	2008	T31	437954.40	856203.05	48.05	0.18	forest	conif	775.96
2008/T33	2008	T33	406517.65	855678.26	48.61	0.18	forest	conif	635.38
2008/T51	2008	T51	429157.31	853468.46	56.49	0.18	forest	decid	777.22
2008/T52	2008	T52	457489.97	867890.79	84.95	0.17	forest	conif	1181.55
2008/T53	2008	T53	457871.26	863687.19	78.55	0.18	forest	conif	1063.63
2008/T54	2008	T54	488781.40	834711.70	48.82	0.17	forest	conif	799.62
2008/T15	2008	T15	478554.51	842612.72	50.12	0.17	forest	conif	770.82
2008/T25	2008	T25	461261.15	852316.31	48.17	0.18	forest	conif	744.09
2008/T55	2008	T55	453931.68	857109.98	26.66	0.21	lake	water	694.00
2008/T34	2008	T34	365790.66	857402.69	50.62	0.17	forest	conif	630.70
2008/T56	2008	T56	340629.37	847327.27	30.38	0.18	forest	decid	576.07
2008/T38	2008	T38	329725.61	842339.10	43.01	0.18	forest	conif	553.45
2008/T40	2008	T40	312911.59	849490.74	45.80	0.18	forest	conif	535.95
2008/T41	2008	T41	302504.99	856562.31	43.65	0.17	forest	conif	657.12
2008/T59	2008	T59	303064.00	842039.96	44.44	0.18	grass	decid	563.09
2008/T57	2008	T57	351494.36	702451.78	50.73	0.18	forest	decid	860.86
2008/T58	2008	T58	361130.29	696692.41	42.97	0.23	forest	water	801.21

Table D.3: Summarized field data, part 2a

	year	mergetrans	x	y	sd	density.pred	lc_field	lc_sat	elev
2009/T45	2009	T45	367412.42	1531681.42	74.48	0.22	bare	conif	1289.64
2009/T46	2009	T46	307981.84	703528.09	64.47	0.18	burn	decid	695.57
2009/T47	2009	T47	319205.89	709972.30	53.33	0.18	burn	burn	681.17
2009/T12	2009	T12	366269.97	689306.88	68.58	0.16	forest	conif	881.98
2009/T05	2009	T05	354525.38	734295.24	23.01	0.21	lake	water	627.00
2009/T1013	2009	T1013	344271.71	746422.14	46.16	0.19	forest	conif	788.92
2009/T1015	2009	T1015	332861.61	763141.66	68.36	0.17	burn	burn	830.00
2009/T1016	2009	T1016	300608.16	851735.90	52.94	0.18	forest	conif	547.06
2009/T49	2009	T49	328773.88	772703.12	73.24	0.19	burn	burn	910.52
2009/T48	2009	T48	324357.32	780551.76	56.93	0.18	forest	conif	698.63
2009/T03	2009	T03	318622.30	805115.46	32.05	0.21	lake	water	627.23
2009/T59	2009	T59	303102.26	841975.02	65.40	0.18	marsh	decid	562.98
2009/T1020	2009	T1020	294238.46	932241.62	58.22	0.18	forest	decid	476.39
2009/T1021	2009	T1021	289831.49	926141.59	47.84	0.21	lake	water	572.36
2009/T1022	2009	T1022	277224.63	910062.76	66.12	0.18	burn	burn	545.00
2009/T41	2009	T41	302353.51	856188.28	51.48	0.17	forest	burn	631.52
2009/T40	2009	T40	313047.00	849532.33	52.01	0.18	forest	conif	537.09
2009/T56	2009	T56	340618.87	847327.06	57.53	0.18	forest	decid	575.51
2009/T50	2009	T50	463374.53	864103.81	98.43	0.20	forest	conif	1326.33
2009/T52	2009	T52	456908.81	867162.47	81.08	0.17	forest	conif	1101.17
2009/T1031	2009	T1031	500498.96	830263.21	42.20	0.20	lake	water	778.78
2009/T1032	2009	T1032	482499.40	839566.09	60.86	0.18	forest	conif	766.11
2009/T1033	2009	T1033	387805.52	858265.03	70.91	0.21	forest	decid	766.97

Table D.4: Summarized field data, part 2b